FACULTY OF SCIENCE AND TECHNOLOGY

MASTER'S THESIS

Study programme/specialisation: Marine and Offshore Technology	Spring semester, 2021. Open/ Confidential
Author: Olatunbosun Bolaji Oluwafemi	
Programme coordinator: Supervisor: Assoc. Prof. Charlotte Obhrai	
Title of master's thesis: Accurate Predictions of Ultimate Limit State Wave Loads on Bottom Fixed Wind Turbine.	
Credits: 30	
Keywords: Wave Breaking, Wave–structure Interactions, Wave Load, Ultimate Limit State.	Number of pages: ……78…….. +supplemental material/other: …… Stavanger, …….11th of June 2021…… date/year

Abstract

The breaking wave loads on a bottom fixed monopile foundation has been determined in this project with the aid of a Pressure Impulse Method. The pressure impulse method is the integration of pressure bounded by time within the period of a short time scale impact. A model implemented on MATLAB as an m-file was derived for an idealized wave on a cylinder with azimuth limits with relative length and impact height. Some model parameters of interest were investigated for their influence on the behavior of the structure. The pressure impulse is confined in the upper layer in both the CFD and model outcomes, which is connected to the little breaker height proportion. The model outcome depends on an attack of θmax to coordinate with the impulse pressure. The acting force increases as the azimuthal point limit increases up until $\pi/2$ where it reaches its peak.

Acknowledgement

I would like to appreciate my supervisor, Assoc. Prof. Charlotte Obhrai. I acknowledge her efforts towards the completion of this thesis. I am grateful for her academic support throughout the year.

I also want to appreciate my wife for standing by me through the whole programme. I acknowledge her support in all ramifications of life.

Table of Contents

Abstract 2
Acknowledgement 3
List of Figures 5
1. **INTRODUCTION** 7
2. **BACKGROUND** 12
2.1 Wave Models and Hydrodynamic Load Computations 12
2.2 CFD Displaying of Water Waves Sway on Surface Slamming Cylinders 12
2.3 The Pressure Impulse Model 18
2.4 Wave Forces on a Vertical Cylinder 19
2.5 Effect of Wave Forces on a Cylinder of Little Diameter 23
2.6 Impact of Wave Powers on a Cylinder with Large Diameter 24
3. **MATHEMATICAL FORMULATION** 28
3.1 Waves Fluid Dynamics 28
3.2 Criteria for Breaking Waves 34
3.3 Slamming Waves 36
3.4 Validation of the Model 39
4. **RESULT AND ANALYSIS** 44
5. **DISCUSSION** 61
6. **CONCLUSION** 61
REFERENCES 62

List of Figures

Figure 3.1 Illustration of Wagner's formulation

Figure. 3.2 Curl effect

Figure 3.3: Definition sketch for 3D block impact on a vertical wall

Figure. 3.4 Axisymmetric impact on a vertical cylinder

Figure 4.1: Pressure impulse of a finite-width fluid block on a flat vertical plate at $\mu = 0.5$, $\frac{b}{H} = 1$, and $\frac{W}{H} = 0.5$

Figure 4.2: Pressure impulse as a function of width of the impacting block, plotted at the mid-height on the flat wall at $z/H = -\mu/2$ and $x/H = 0$

Figure 4.3: Pressure impulse as a function of width of the impacting block, plotted at the mid-width on the flat wall at $y/W = 0$, $x/H = 0$

Figure 4.4: Pressure impulse as a function of width of the impacting block, plotted at the mid-height on the flat wall at $z/H = -\mu/2$ and $x/H = 0$

Figure 4.5: Pressure impulse of a finite-width fluid block on a flat vertical plate at $\frac{W}{H} = 0.2$

Figure 4.6: Pressure impulse of a finite-width fluid block on a flat vertical plate at $\frac{W}{H} = 0.4$

Figure 4.7: Pressure impulse of a finite-width fluid block on a flat vertical plate at $\frac{W}{H} = 0.4$

Figure 4.8: Pressure impulse as a function of width of the impacting block, plotted at the mid-width on the flat wall at $y/W = 0$, $x/H = 0$

Figure 4.9: Dimensionless pressure impulse on the inner cylinder, at $\theta = 0$, plotted as a function of z/H for several values of μ.

Figure 4.10: Dimensionless pressure impulse on the inner cylinder, at $\theta = 0$, plotted as a function of z/H, (a) for several values of b/H

Figure 4.11: Dimensionless pressure impulse on the inner cylinder plotted (a) as a function of z/H, at $\theta = 0$, for several values of a/b.

1. **INTRODUCTION**

The greatest test confronting the human species is right now the ecological danger from the worldwide temperature boost. The best arrangement researchers have to think of is to restrict fossil fuel utilization to the barest minimum and replace the non-environmentally friendly power source with renewable ones, for example, solar, hydro, and wind energy. This progress of replacing fossil fuel with clean energy emphatically have a strong hold on the economy on a global scale (Ferroukhi et al. 2017). Subsequently, the Danish government, for instance, has a set goal of meeting half of Denmark's energy demand with renewable energy in 2030 and completely eliminate petroleum derivatives by 2050 (International Energy Agency 2017). The popular understanding among driving researchers is that a worldwide temperature alteration represents a genuine ecological danger. One approach to mitigate the results of an increase in the global temperature is to change the universe's energy supply from petroleum derivatives to clean energy such as solar, hydro-and wind energy. To agree with this, the Danish government chose in 2012 that the portion of energy created from renewable energy sources should increase from 18.9% to 50% by 2020.

One of the developing environmentally friendly renewable energy during the most recent decade has been the wind energy. In Denmark, the normal wind speed at a height of 100 meters is somewhere in the range of 6 and 10 m/s while the normal offshore wind speed is between 9 and 11 m/s. In 2012, Denmark put forward an objective so that by 2020, half of the power utilization ought to be provided by wind power. Wind energy was at that point giving 42% of the power utilization in 2016 and is required to give 48% of the power by 2020 (International Energy Agency 2017). So, it is expected that wind energy keeps on being the essential environmentally friendly energy source in Denmark. In 2015, the Danish Energy Agency performed a feasibility study,

which exhibited that it is conceivable to plan energy frameworks, comprising of just environmentally friendly energy source, free of petroleum products (International Energy Agency 2017). There is a bigger expected limit in offshore in respect of uninhabited body parts and higher normal wind speeds. Also, the wind environment is steadier offshore. Bigger wind turbines can be introduced offshore and there are fewer or no objections from districts and adjoining residents. Denmark has more than 7300 km of coastline with low normal ocean width which is ideal for offshore wind energy. Information shows that the interest in offshore wind energy is expanding more quickly than inland wind energy (REN21 2017). Recent information additionally shows that the expense of offshore is diminishing in the Danish market which is delicately driven. Amongst the various plans of construction for offshore wind turbines, monopiles are the most utilized in terms of its simple design and construction.

Normally, wind energy will be the fundamental contributor as this type of environmentally friendly energy source is exceptionally appropriate for the Danish climate and the political plan. The expansion plan is to replace existing turbines with new, bigger, and more productive ones. Normally, a critical piece of all new wind turbines will be introduced offshore. Before the year 2012, 1,662 ocean wind turbines were introduced and lattice associated in Europe, giving a complete generation of 5.00 GW. It is expected that before the year 2014, the generation will increase by a further 3.30 GW (Arapogianni, 2013). The monopile-tower type structure has created wide interest as of late and a favoured base to help solve the problem associated with fixed offshore wind turbines at shallow water. An offshore wind turbine introduced on monopiles foundations requires an accurately assessed extreme load state (ULS) exuding from complex wave load to prevent loads failure. As indicated by Hull and Muller (2002), the breaking wave in ocean is a significant concern, inferable from the unpredictable circumstance of the wave breaking

impact and the breaking wave time series. Oggiano et al. (2017) in their investigation announced that the Computational Fluid Dynamics strategy was utilized to repeat the work carried out from the WaveLoads exploratory mission. Huge speed increases at nacelle level in breaking waves was explained by Ridder et al. (1998), they announced the significance of examining the unique conduct of an offshore wind turbine structure while Rogers (2011) examined an offshore wind turbine structure with just the breaking waves experienced. The wave around two vertical cylinders, utilizing a 3D Navier-Stokes solver dependent on the FDM was studied by Lee et al. (2011). They utilized the VOF strategy to represent the free surface. They noted that there is a decent arrangement between the mathematical outcomes and the trial estimations. A 3D mathematical model dependent on the FDM was used by Choi (2014) to reenact the breaking wave on a vertical cylinder pile while the VOF technique was utilized to determine the air-water interface. A wave breaking over an inclining seabed was discussed by Chella et al. (2016), they used a mathematical model which depends on Reynolds number and solved the midpoint of Navier-Stokes conditions combined with the level set strategy. There is an excellent agreement between the numerical result and the test estimations as revealed by Ting and Kirby (1996). Paulsen (2013) coupled the OpenFOAM with a potential stream solver to research the wave in a vertical cylinder. The outcome showed a magnificent agreement with the exploratory estimations. Over the years, additional opportunities for a better exact assessment of the limit waves and their piles have been given because of advances in mathematical wave hydrodynamics. A lot of investigations have been carried out on breaking wave with a vertical tube-shaped construction with numerous vulnerabilities. A detailed information on the cycle will prompt an improvement in the plan and enhancement of the design. Mathematical models help in the assessment of the effect of tension on offshore constructions for better comprehension of the problem. The utilization

of mathematical models in wave hypothesis gives a precise depiction of how the water surface acts comparable to the monopile structure. The major objective of the study is to compute breaking wave loads on-base fixed monopile construction utilizing Non-linear Wave Kinematics and Pressure Impulse methods. Monopile are cylinders fixed into the ocean bed slamming the outside of the water. A piece at the highest point of the monopile interfaces the monopile and the wind turbine tower. Large-scale manufacturing of monopile construction is simple, which makes monopiles the most expense-effective sort of construction for offshore wind turbines at width up to 40 m. Over 80% of the grid-connected offshore wind turbines are introduced on monopiles. One hindrance of the monopile constructions is their little primary strength and underlying damping on account of their thin shape. To increase the strength in bigger water width (longer monopiles), the distance across ought to be expanded which infers more costly bases. Consequently, the utilization of complex waves and the related Ultimate Limit State (ULS) loads can be factor in for planning the boundaries of the monopile. To diminish the expense of offshore wind energy, Megavind (2013) came up with improved plan models which reduces the associated hazards and failure of key components. The construction of offshore wind turbines regularly makes out 20% of the absolute expense of energy (Technology Innovation Needs Assessment (TINA) 2012). Subsequently, a decrease in failure of monopile configuration can play a significant part in the offshore wind energy cost decrease. At present, basic techniques utilized in the business for wave load forecast on offshore wind support structures are portrayed in the IEC 61400-3 (2009) plan code among different handbooks. The techniques are started in the oil and gas industry expecting a level bed. In these strategies, complex waves are addressed by ordinary wave arrangements. The actual impacts of wave nonlinearity, 3D impacts, and wave-current connection are, consequently, barred from these techniques. The pile estimations in these techniques are to a great extent

dependent on the understanding that the limit wave stacking is related to the biggest breaking wave.

2. **BACKGROUND**

2.1 Wave Models and Hydrodynamic Load Computations

The current suggested practice for estimation of hydrodynamic loads, counting the ULS cases, is introduced in IEC 61400-3 (2009). The initial step to figuring the hydrodynamic loads is to pick the suitable wave model. The distinctive wave speculations give answers for similar differential conditions and limit conditions with various solutions. If the linear wave hypothesis is chosen to compute the wave kinematics, extending strategies, for example, Wheeler or Delta technique ought to be utilized to ascertain the kinematics from the still water level to the free surface. Morison's condition (Morison 1953) is utilized to compute the hydrodynamic powers from the wave kinematics determined from the proper wave hypothesis.

2.2 CFD Displaying of Water Waves Sway on Surface Slamming Cylinders

Christensen, Bredmose, furthermore, Hansen (2005) studied the wave run-up and inline powers on offshore. Wind turbines utilizing in-built program created Navier Stokes solver called NS3, the run-up and powers on the monopile are unequivocally impacted by the breaking cycle. They used the model with estimations directed by Kriebel (1992) for non-breaking and breaking waves. The calculations were completed with a slip limit condition at the cylinder wall. Bredmose et al. (2006) expanded the examination for the limit wave loads on offshore wind turbines in an unpredictable ocean state. Later Bredmose and Jacobsen (2010) explored breaking wave impacts from centered wave gatherings on offshore wind turbine monopiles utilizing OpenFOAM and approved the mathematical model with direct wave driving. In expansion, Bredmose and Jacobsen (2011) researched wave impacts on offshore wind turbine and represented the capability of CFD estimations for rough wave loads. They announced that the regular recurrence of the construction may be energized during the wave impacts on the assessment stages.

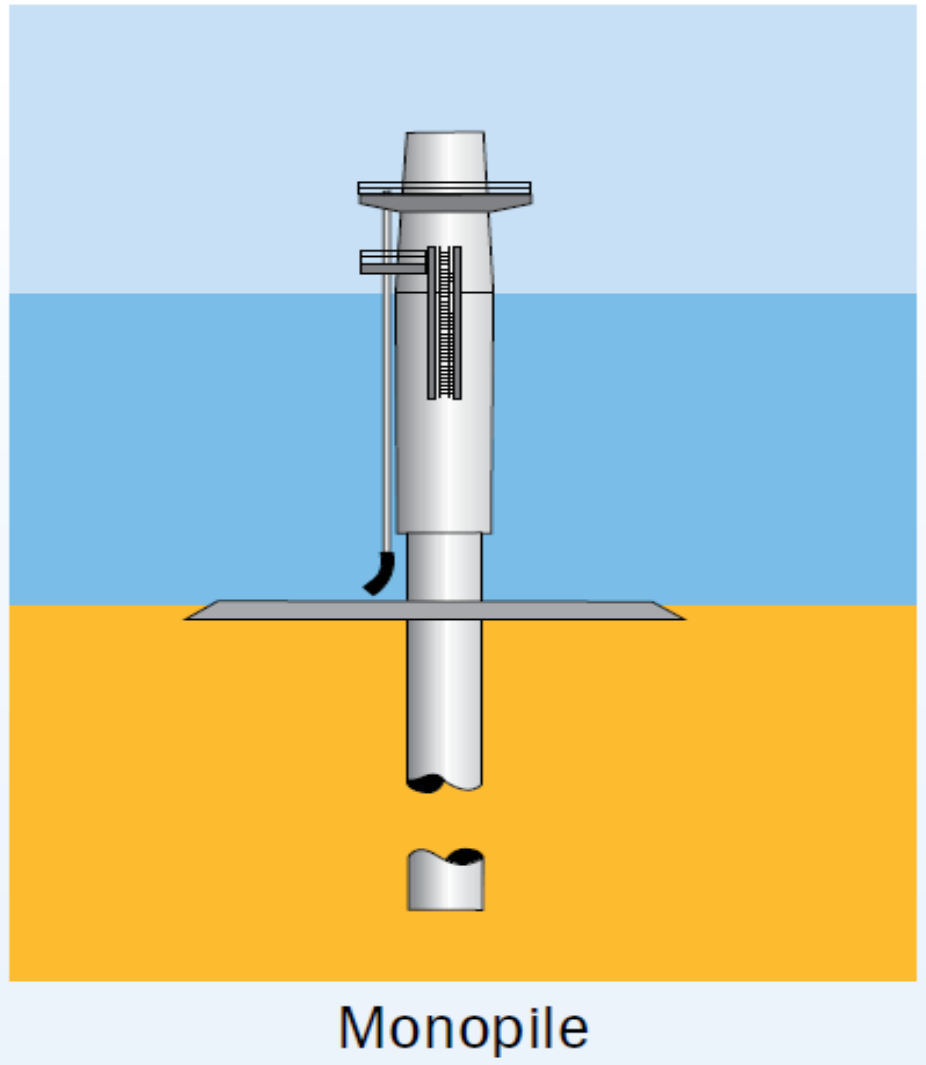

Fig. 2.1: A monopile structure (google.com, 2021)

Filip and Maki (2015) utilized Large Eddy Simulations (LES) to demonstrate the powers from the free surface progression of steep non-breaking standard waves and approved them with tests. They broadened the examination by displaying breaking waves and showed that the expectation of powers on a vertical round cylinder is improved by the utilization of the all-encompassing LES model for multiphase free surface stream utilizing the Volume of Fluid technique. Filip (2013) was one of the first to consider the impacts for computation of the wave powers on a superficial penetrating cylinder. Bingham (2014) created and introduced aftereffects of the space decay

strategy for demonstrating wave loads on surface penetrating cylinders. They showed that the strategy functions admirably by approving broadly against all tests. The cases included breaking and non-breaking waves. Furthermore, they were the first to report the proliferation of the Secondary Load Cycle in the mathematical outcomes. Paulsen et al. (2014) at that point provided additional information on the examination of the stream structure connection and suggested constraining of a base mounted round cylinder by steep water waves at limited diameter. They particularly provided more explanation on the Secondary Load Cycle in the inline power history. The mathematical outcomes agree excellently with the test estimations of the non-breaking customary waves. Although they examined the surrounding stream around the cylinder, its limit layer was neither settled nor demonstrated. Chen et al. (2014) examined the effect of OpenFOAM when applied to Non-linear wave with offshore constructions for 4 instances of normal and 4 instances of sporadic stage-centered wave gatherings. They concluded that the OpenFOAM is suitable for solving the nonlinear waves.

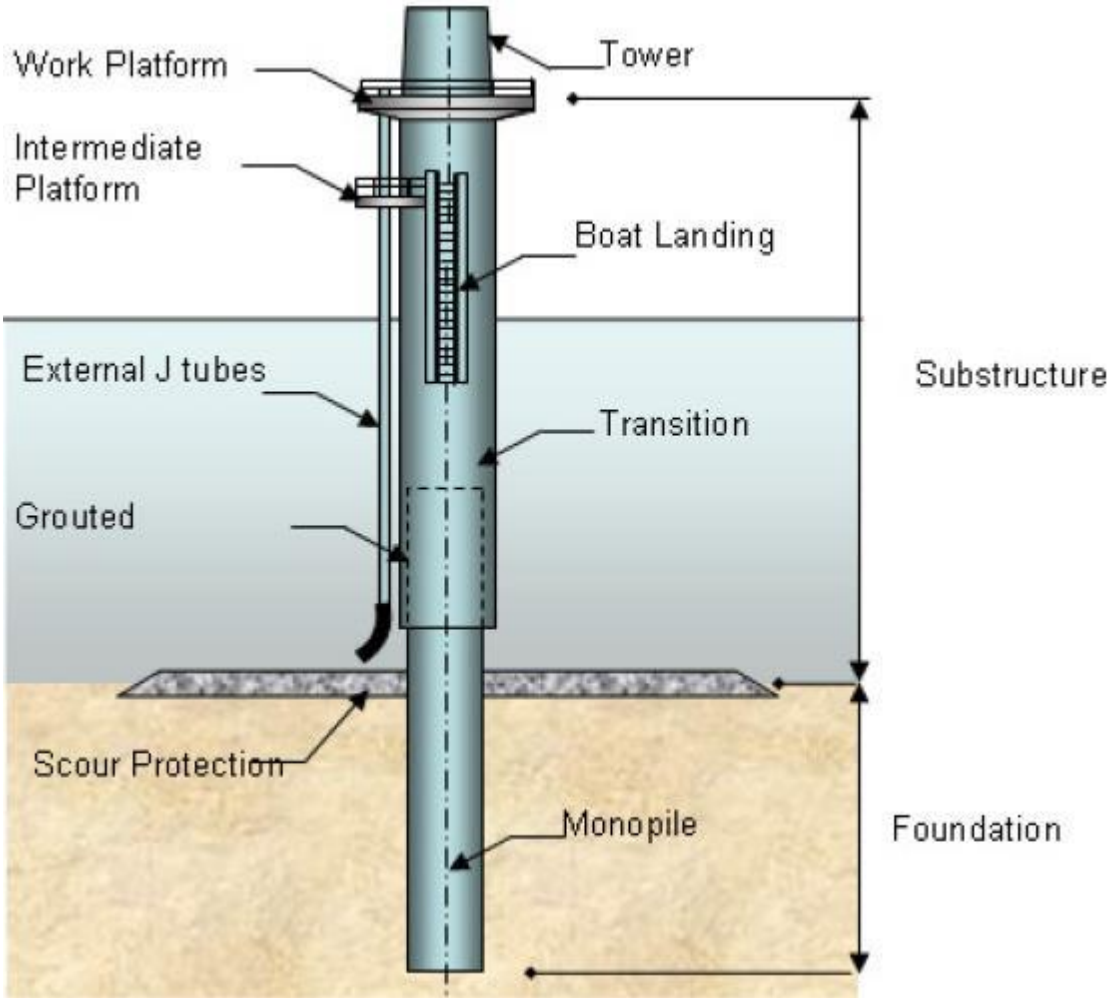

Figure 1.2 Monopile structural foundation (Leite, 2015)

The investigation included in-built force, free surface height, the optional load cycle and in-built power time series. This investigation was the main mathematical examination of waves and monopile cooperation including a no-slip limit adapted monopile.

Hildebrandt and Sriram (2014) investigated the pressure impulse dispersion and vortex shedding around a cylinder because of a precarious non-breaking wave utilizing estimations and mathematical displaying. The pressure impulse was estimated on the outside of the cylinder in various heights and azimuths and compared to the mathematical results. The model used in the

study was an ANSYS-CFX with Reynolds Averaged kω-SST. They presumed that the model is reasonable for surrounding stream around a surface piercing cylinder in waves. Choi *et.al* (2015) utilized the unique enhancement strategy to represent the reaction of the construction because of breaking wave impacts. The paper showed that they created a 3D mathematical model that performs well in displaying the breaking wave and creating dependable results including approximated structure reaction.

Fig.2.3: Bottom fixed foundations for wind turbines (google.com. 2021)

A created Navier Stokes solver, REEF3D, was utilized by Alagan Chella (2016) to reproduce the free surface waves and to direct a point-by-point examination of the state of the wave breaker and surrounding fluid around the cylinder. The model was approved by correlation with tests of breaking waves on a slanted bed. They detailed the pile of a water segment (hill) behind the cylinder and related it to the diameter of water. The cylinder wall incorporated a no-slip limit condition with wall capacities to represent the upsides of k and ω in the kω disturbance model.

Devolder *et al* (2017) broadened and applied a buoyancy modified kω-SST disturbance model to recreate wave run-up around a monopile exposed to standard waves utilizing OpenFOAM. They showed that utilization of adjusted kω-SST expands the consistency of the mathematical techniques to moderate the state of standard waves. At that point, they utilized this to ascertain the run-up tests. The included wave cases were non-breaking and the limit layer on the cylinder wall was demonstrated utilizing wall capacities. Jose et al. (2017) studied the mathematical models of breaking wave powers on a monopile structure, utilizing the limited volume models. They utilized a strategy to refine the lattice around the free surface height locally. They noted that the auxiliary load cycle is brought about by the hydrostatic impact of the water segment. A decent consistency of the mathematical outcomes appears in this work with a kω-SST disturbance model tests for both mathematical models. Veic and Sulisz (2018) broke down the effect of pressure dissemination on a monopile structure energized by two sporadic breaking wave scenes. They explained the comparable systems of the breaking wave, in pressure circulation and in both effect cases and showed that the worth of the top slamming coefficient is around equivalent to $Cs = 2\pi$. They introduced the impulse pressure on the cylinder during the pummelling. The auxiliary load cycle in the mathematical model time history of free surface waves communicating with a surface penetrating cylinder was first revealed by Paulsen *et al.* (2014) and afterward revealed by various

researchers utilizing the diverse mathematical models. Utilizing a no-slip limit condition on the cylinder wall was first and foremost fused by Chen et al. (2014) and right up 'til today has been used a couple of times. Be that as it may, the use of LES models has not been applied from that point forward and just RANS type models, particularly kω-SST, have been utilized a couple of times.

2.3 The Pressure Impulse Model

The slamming force from waves is frequently displayed with the Wienke and Oumeraci model (2005). The precision of this model has frequently been evaluated as far as most extreme pressure. For structural modes with high recurrence, the primary reaction is based on the force impulse theory instead of the peak force value. Thus, even with a solid expectation of the peak force value, the reaction will in any case rely upon a precise depiction of the effect time scale. A less complex way to deal with the slamming force may along these lines be acquired by direct displaying of the time coordinated pressure. The model of Ghadirian and Bredmose executes this methodology by utilizing a shut structure answer for a limit characterized by linear wave boundaries. The spatial dissemination of the pressure impulse is in this manner part of the arrangement. The affecting wave is depicted in a calculated solution. The area is wedge-shaped with azimuth limits $-\theta max \leq \theta \leq \theta max$ and comprises of at first moving and still liquid above and underneath $z = -\mu H$ individually. Here H is the vertical separation from the bed to the free surface for the wave at the underlying effect and μH is the height of the effect zone. Until before the impact period, the upper part is moving toward the cylinder with speed U in the negative x ($r \cos\theta$) heading. At the limits $\theta = \pm\theta max$, $z = 0$ and $r = b$ the condition $P = 0$ must be fulfilled.

2.4 Wave Forces on a Vertical Cylinder

The turbine monopile support section is depicted as a vertical smooth, surface-slamming, fixed cylindrical structure. The local hydrodynamic system relies upon the episode wave boundaries, water diameter, and length size of the cylindrical structure. No strategy exists that is generally relevant for anticipating the wave stacking on a surface piercing structure under all conditions; the length size of the structure, wave period, thickness, and different elements should be considered to decide the impact that the presence of the structure has on the passing water stream (Dean and Dalrymple, 1991). The overall force is subject to the liquid stream system, depicted as far as the parameters recognized, and the relative size of the cylinder distance across the diameter to the frequency λ. For little distance across structures where the measurement to-frequency proportion $D/\lambda < 0.2$, it could be expected that the presence of the structure negligibly affects the impulse pressure of the slamming waves. As the structure measurement to-frequency proportion builds, the presence of the structure alters the local hydrodynamic impulse pressure slope and the latency pressure, which is the pressure because of energy, expands. In the system, where both drag and dormancy pressures are significant, both thick and diffraction pressure parts add to wave stacking, and the stream can encounter extra impacts because of wave nonlinearity within the sight of high-recurrence diffracted waves (Swan and Sheik, 2014).

In coastal engineering, Goda *et al* (1966) is mostly used to determine the impact force on monopiles due to breaking waves.

$$F_1(t) = \lambda.\eta_b.\ \pi.\ \rho.\ R.\ C^2\ (1 - \frac{C}{R}t) \qquad (2.1)$$

Where:

$\lambda.\eta_b$ = the height of the impact area

C = celerity of the wave

η_b = the crest height of the breaking wave

λ = the curling factor

R= radius of the cylinder

ρ = density of the fluid

$$F_1(t) = \pi.\ \rho.\ R.\ V^2\ (1 - \frac{C}{R}t) \quad (2.2)$$

Where C = V

$$F_1 = \pi.\ \rho.\ R.\ V^2 \quad (2.3)$$

$$F_1 = C_s.\ \rho.\ R.\ V^2 \quad (2.4)$$

The pressure impulse model for slamming wave on a vertical wall can be determined using the expression shown below:

$$\frac{P}{\rho UH}(\frac{x}{H}, \frac{y}{W}, \frac{z}{H}) = f(\frac{b}{H}, \mu, \frac{W}{H}) \quad (2.5)$$

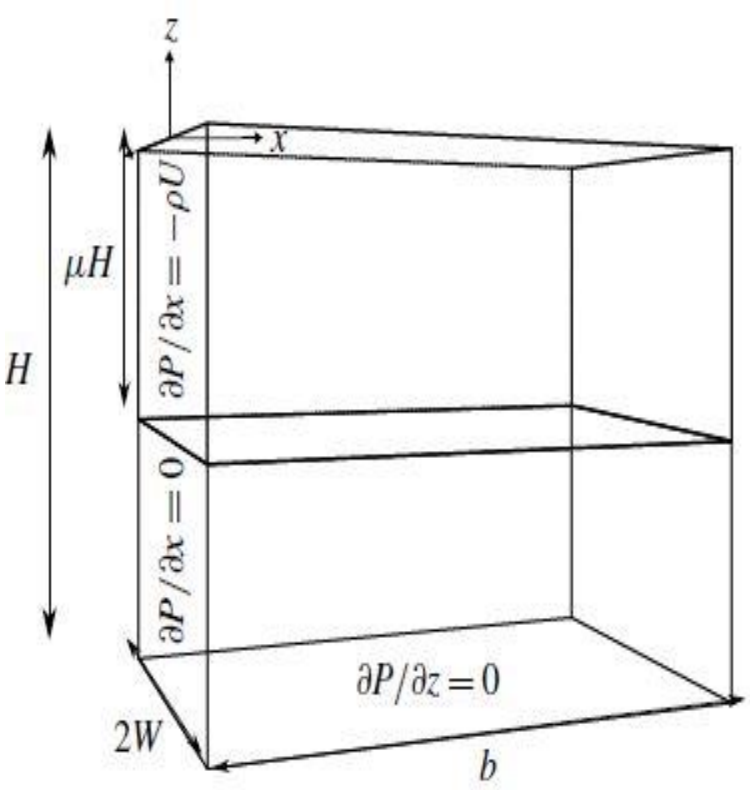

Fig. 2.4: Definition sketch for 3D block impact on a vertical wall (Ghadrian and Bredmose, 2019)

Where $\frac{b}{H}$ represent the relative length of the block

$\frac{W}{H}$ represents the relative width of the block

μ represent the relative height of the impacting zone

The vertical wall is located at x=0, during impact, the vertical wall was impacted by the fluid at a normal velocity U bounded within $-\mu H \leq z \leq 0$.

The application of the separation of variable method and Fourier series to eqn.4 analysis yields

$$P(x,y,z) = \sum_{m=1}^{\infty}\sum_{n=1}^{\infty}\left(\left(A_{mn}\cos L_m\frac{y}{W}\right)\sin\left(K_n\frac{z}{H}\right)\frac{\sinh\left(\sqrt{L_m^2(\frac{H}{W})^2+k_n^2}\left(\frac{b}{H}-\frac{x}{H}\right)\right)}{\cosh\left(\sqrt{L_m^2(\frac{H}{W})^2+k_n^2}\left(\frac{b}{H}\right)\right)}\right)$$

(2.6)

Where $L_m = \left(m-\frac{1}{2}\right)\pi$

$K_n = \left(n-\frac{1}{2}\right)\pi$

$$A_{mn} = 4\rho UH\frac{(COS(k_{n\mu})-1)\sin(L_m)}{\cosh\left(\sqrt{L_m^2(\frac{H}{W})^2+k_n^2}\right)} \quad (2.7)$$

The Reynolds number (Re) and the Keulegan-Carpenter number (KC) are generally used to depict the proportion of idleness to-thick pressures and the proportion of drag-to-inactivity pressures separately, for a liquid stream past a snag (Faltinsen, 1990, Sarpkaya and Isaacson, 1981). Zdravkovich (1997) has ordered a unidirectional stream past a cylinder and gave the stream portrayals with expanding Re, the liquid stream changes from a laminar stream with no partition at the structure surface to a completely violent stream, where the stream movements are rotational. As the impulse pressure slope diminishes, the vortices separate from the structure and travel downstream, making a wake or a vortex design (Sumer and Fredsøe, 2006). The all-out in-line wave power on a vertical surface-penetrating fixed cylinder in since quite a while ago peaked waves can be ascribed to the unstable impulse pressure field inside the episode wave field over the lowered cylinder length (Dean and Dalrymple, 1991). In an ideal potential stream where it is accepted that the cylinder has no impact on the stream field, the complete in-line pressure per unit height can be determined as the amount of the drag power (Fp, D). In an expected stream, the lift

power part is equivalent to nothing. Nonetheless, in a wave field, when the episode wave peak passes, the wave box arrives at the turbine, the stream field is switched and the wake returns towards the turbine, bringing about the pressure stacking turning around bearing. The directional changes and stream divisions break the earlier suppositions of an irrotational stream and an inviscid liquid accepted by the expected hypothesis (Dean and Dalrymple, 1991), and the impulse pressure incorporations are not equivalent to nothing. This deviation from the normal outcome in an even stream is called D'Alembert's Paradox, which happens because of the presumption of a potential irrotational stream (Dean and Dalrymple, 1991). Two more surmised techniques are utilized to figure the wave force on a monopile, contingent upon the structure diameter to-frequency proportion: one for little breadth structure and the other for enormous measurement structures. In the accompanying segments, the force computations depend on the fact that the wave field involved is direct waves in either a standard wavefield with a solitary modular wave recurrence or in an unpredictable unidirectional wavefield with a scope of wave frequencies.

2.5 Effect of Wave Forces on a Cylinder of Little Diameter

It is accepted that the flow near the structure is not changed in the occurrence wave bearing, the Morison condition is ordinarily used to appraise the absolute in-line pressure (Morison et al., 1950). The Morison condition involves the straight amount of drag and latency pressure segments and is assessed by utilizing the undisturbed water speed and speed increase segments determined without the structure. The additional mass pressure results from the power of the fluid following up on the lowered piece of the construction. Thick impacts in the limit layer on the structure wall actuate stream detachment prompting the arrangement of a vortex road wake at $KC > 3$ (Faltinsen, 1990). The drag (Cd) and idleness (Cm) coefficients are normally decided tentatively. Results from numerous exploratory tests have been accumulated and acknowledged at a scope of Re qualities

for a smooth structure. Around Re > 10^5, it very well may be seen that there is a drop in the Cd worth before it increases once more.

2.6 Impact of Wave Powers on a Cylinder with Large Diameter

Direct diffraction hypothesis applies to wave stream past an enormous measurement cylindrical structure when the proportion of the breadth to-frequency ≥ 0.2. In this reach, diffracted waves are created by a mix of waves reflected from the cylindrical and the undisturbed episode wave field. The underlying undisturbed episode wave field potential can be written in complex documentation, utilizing polar directions (r, θ) in the level plane, the occurrence wave potential that fulfills the polar type of Laplace's condition and the kinematic and dynamic free surface limit conditions (MacCamy and Fuchs, 1954) is given in the standard structure with a Bessel work. As the occurrence wave impacts upon the structure, a reflected wave is emanated outwards and communicates with the wave. Joining the undisturbed occurrence likely φI and a dispersed potential, the study got an insightful answer for the diffracted speed potential with the consideration of a Bessel function within the cylindrical structure range. On the structure wall, the outspread separation from the focal point of the segment is r = R. By definition, z = rcosθ, where θ alludes to the area on the cylinder as estimated against clockwise from the middle line toward a stream. The diffracted surface rise ηD is found from the linearised Bernoulli condition and applying the diffracted potential gives the straight diffracted surface rise as ηD = a. Standard diffraction investigation expects ordinary monochromatic waves and can overestimate wave heights nearby an impediment in a given ocean state (Goda, 1985). The diffracted wave height in an unpredictable wave field is gotten from the superposition of the diffracted wave arrangement got for every individual wave segment, where frequencies of the radially outward moving diffracted waves relate to frequencies of the episode waves (Swan and Sheik, 2014). It ought to be

focused on that the condition is just legitimate for straight diffracted waves, thus does not hold when nonlinear diffraction gets critical. The sporadic diffracted water molecule kinematics, uD, and wD can be resolved to ascertain the individual diffracted amplitudes from the diffracted wave range. The absolute wave power on an enormous measurement structure can likewise be resolved from the diffraction hypothesis. The in-line power can be resolved through a combination of the surface impulse pressure. The impulse pressure field would then be able to be acquired from the Bernoulli condition and the subsequent in-line diffracted power per unit length given by MacCamy and Fuchs (1954) where the absolute diffraction power can be found through the incorporation of the condition vertical along the lowered length of the structure. Essentially, the unpredictable in-line diffracted power can be communicated as the amount of every individual diffracted wave power segment. The diffracted power range can be found by a similar technique where the diffracted power range can be controlled by FFT of the diffracted power, where again Fs is the examining recurrence and N are the numbers of recurrence receptacles. It should be noticed that the diffraction strategy just purposes the first-order terms and ignores higher-request terms, the upsides of which can be non-irrelevant. Upgrades to the techniques above could be made by endeavouring to decide higher-request diffraction terms utilizing a strategy, for example, that introduced by Chau and Taylor (1992).

2.7 Wave Generation

Gaussian wave packets were utilized to empower wave breaking at a given area in the wave flume (Bergmann, 1985). Now, the wave turns out to be exceptionally steep and breaking should proceed. Thusly, the wave separates. The spreading of the wave in the wave flume for three diverse time steps. The determined wave has a focus ways off of 111m from the wave paddle and the surface rise now is 1.5m with plunging breakers created. All produced waves were very comparable in the

area of breaking. The celerity C of the breaking wave was around 6 m/s, the wave time frame T was about 4.2 s, and the wave height Hb differed between 2.2m and 2.8m. The state of the waves at the limit was awry according to both the even plane (l=gb/Hb) and the vertical plane (kV= LW/LV). Contrasting these wave shapes as expressed in field estimations (Kjeldsen, 1990), shows excellent agreement. The wave box in the flume is more particular, with the goal that the boundary l portraying the flat unevenness is more modest. The worth of the vertical imbalance factor kV is bigger suggesting that the front of the wave peak is more extreme than the backside. So ideally, the wave does not replicate normal breaking waves in ocean water, however, they address a helpful strategy to create breaking waves at given areas in a wave flume for the investigation of the effect on structures.

The breaking wave on the vertical and slanted thin cylinder was analysed by a progression of largescale model trials utilizing Gaussian wave bundles to produce a tailored plunging breaker at given areas in the enormous wave flume. The age of single wave occasions for each test permitted to accomplish a high goal of the effect pressures (0.1 ms) and the utilization of huge scope tests permitted to a great extent stay away from scale impacts related with the effective power. The breaking wave was investigated by partitioning the pile into a semi-static and powerful segment. The semi-static power is very much depicted by the Morison condition, while for the unique part no dependable methodology is accessible which is in full concurrence with the perceptions. It was tentatively shown that the effect pressure improvement can be addressed by a spiral spreading around the main contact point. The advancement of the breaking wave at the cylinder was researched both hypothetically and tentatively. In light of the two-dimensional depiction of Wagner (1932), which has been confirmed tentatively in this investigation, the complete term of

the effect was resolved. The effect begins with the main contact between the cylinder and the impinging mass of water.

2.8 Wind Load

Drag loads of the wind that act on a vessel are results of the fluid's relative velocity. Since that the structure is correlated with energy produced from the wind, the loads are expected to be significant. Wind loads have a direct relationship with the areas subjected to the flow.

2.9 Wave Physics

An intensive comprehension of the physical science behind the pile is indispensable for a significant way to deal with its demonstrating and definition into a plan. Thus, thorough examinations are done in 3D and 2D conditions. The actual impacts straightforwardly tended to are 3D wave spreading, the impact of wave-current communication, the impact of upgraded base height, and the impact of air-entrainment from wave breaking. PIV estimations of occurrence wave kinematics are made to permit direct approval against mathematical kinematics and to empower approval of pressure models dependent on the episode kinematics. While a considerable lot of the referenced impacts are as of now known and depicted to a specific level, the focal point of the examinations is on the related effect on the hydrodynamic load. The motivation behind the tests is in two-dimension. The tests should archive the monopile impacts independently and include the application of the mathematical models which can afterward be utilized to broaden the boundary space.

3. MATHEMATICAL FORMULATION

3.1 Waves Fluid Dynamics

There is an assumption that a function exists with its gradient representing a fluid flow, this can be expressed mathematically as

$$V = \nabla\emptyset \tag{3.1}$$

The assumed function is referred to as the potential flow. The V in the equation is equal to the total velocity of the fluid flow.

According to Newton's 2nd law which states that force is equal to the product of the mass of an object and the acceleration of the object which is expressed mathematically as;

$$F = M * \alpha \tag{3.2}$$

When this is applied to the mass or body of fluid flowing, the equation becomes:

$$dF = dm * \frac{D\vec{V}}{DT} = dm * [u\frac{\delta\vec{V}}{\delta x} + v\frac{\delta\vec{V}}{\delta y} + w\frac{\delta\vec{V}}{\delta z} + \frac{\delta\vec{V}}{\delta t}] \tag{3.3}$$

The acting forces on a liquid body can be inferred utilizing an expansion method known as Taylor's series. For any course, an amount of the liquid body component forces can be expressed as

$$dF_{S_x} = \left(\frac{\delta\sigma_{xx}}{\delta x} + \frac{\delta\tau_{yx}}{\delta y} + \frac{\delta\tau_{zx}}{\delta z}\right) dxdydz \tag{3.4}$$

Taking gravitational force into consideration, the equation becomes:

$$dF_{S_x} = \left(\rho g_x + \frac{\delta\sigma_{xx}}{\delta x} + \frac{\delta\tau_{yx}}{\delta y} + \frac{\delta\tau_{zx}}{\delta z}\right) dxdydz \tag{3.5}$$

A set of equation for motion is derived when the Newton's 2nd law is substituted for the parameter "dF" in the equation, thus the continuum assumptions is satisfied as expressed below:

$$\rho g_x + \frac{\delta \sigma_{xx}}{\delta x} + \frac{\delta \tau_{yx}}{\delta y} + \frac{\delta \tau_{zx}}{\delta z} = \rho + (u\frac{\delta u}{\delta x} + v\frac{\delta u}{\delta y} + w\frac{\delta u}{\delta z} + \frac{\delta u}{\delta t})$$

$$\rho g_y + \frac{\delta \tau_{xy}}{\delta x} + \frac{\delta \tau_{yy}}{\delta y} + \frac{\delta \tau_{zy}}{\delta z} = \rho(u\frac{\delta v}{\delta x} + v\frac{\delta v}{\delta y} + w\frac{\delta v}{\delta z} + \frac{\delta v}{\delta t}) \quad (3.6)$$

$$\rho g_z + \frac{\delta \tau_{xz}}{\delta x} + \frac{\delta \tau_{yz}}{\delta y} + \frac{\delta \sigma_{zz}}{\delta z} = \rho(u\frac{\delta z}{\delta x} + v\frac{\delta z}{\delta y} + w\frac{\delta z}{\delta z} + \frac{\delta z}{\delta t})$$

$$\rho\left(u\frac{\delta u}{\delta x} + v\frac{\delta u}{\delta y} + w\frac{\delta u}{\delta z} + \frac{\delta u}{\delta t}\right) = \rho g_y - \frac{\delta \rho}{\delta x} + \mu(\frac{\delta^2 u}{\delta x^2} + v\frac{\delta^2 u}{\delta y^2} + \frac{\delta^2 u}{\delta z^2})$$

$$\rho\left(u\frac{\delta u}{\delta x} + v\frac{\delta u}{\delta y} + w\frac{\delta u}{\delta z} + \frac{\delta u}{\delta t}\right) = \rho g_y - \frac{\delta \rho}{\delta y} + \mu(\frac{\delta^2 v}{\delta x^2} + v\frac{\delta^2 v}{\delta y^2} + \frac{\delta^2 v}{\delta z^2}) \quad (3.7)$$

$$\rho\left(u\frac{\delta w}{\delta x} + v\frac{\delta w}{\delta y} + w\frac{\delta w}{\delta z} + \frac{\delta w}{\delta t}\right) = \rho g_z - \frac{\delta \rho}{\delta z} + \mu(\frac{\delta^2 w}{\delta x^2} + v\frac{\delta^2 w}{\delta y^2} + \frac{\delta^2 w}{\delta z^2})$$

Working with the assumption that the friction is zero (= 0), the equation which is Navier-Stokes reduces to Euler's equation as expressed below:

$$\rho\left(u\frac{\delta u}{\delta x} + v\frac{\delta u}{\delta y} + w\frac{\delta u}{\delta z} + \frac{\delta u}{\delta t}\right) = \rho g_y - \frac{\delta \rho}{\delta x}$$

$$\rho\left(u\frac{\delta v}{\delta \mathrm{x}} + v\frac{\delta v}{\delta y} + w\frac{\delta v}{\delta z} + \frac{\delta v}{\delta t}\right) = \rho g_y - \frac{\delta \rho}{\delta y} \quad (3.8)$$

$$\rho\left(u\frac{\delta w}{\delta x} + v\frac{\delta w}{\delta y} + w\frac{\delta w}{\delta z} + \frac{\delta w}{\delta t}\right) = \rho g_z - \frac{\delta \rho}{\delta z}$$

Also, Bernoulli's equation is derived from the Integration of the Navier-Stokes equations which gives the equation below:

$$\frac{p - p_0}{p} = -\emptyset_t - \tfrac{1}{2}(\nabla\emptyset)^2 - gy \quad (3.9)$$

Where ϕ equals the potential flow equation and the derived Bernoulli equation is expressed as:

$$p + \rho g\xi + \rho\frac{\delta\phi}{\delta t} + \frac{1}{2}\rho V * V = C \tag{3.10}$$

The kinematic boundary condition indicates a solid boundary does not allow the passage of fluid through it which is mathematically expressed as:

$$V * n \equiv \frac{\delta\phi}{\delta n} = U * n \tag{3.11}$$

And a free surface expressed as:

$$\zeta = (\xi, \eta, t) \tag{3.12}$$

Where:

ζ: 0 at the surface

ζ: -h at depth h

Implementing the kinematic boundary condition on the free surface formulation gives the following derivative.

$$\frac{\delta f}{\delta t} + \frac{\delta\phi}{\delta\xi}\frac{\delta f}{\delta\xi} + \frac{\delta\phi}{\delta\eta}\frac{\delta f}{\delta\eta} + \frac{\delta\phi}{\delta\zeta} = 0 \qquad on\ \zeta = f \tag{3.13}$$

$$gf + \frac{\delta\phi}{\delta\xi} + \frac{1}{2}V * V = 0 \qquad o\ n \quad \zeta = f \tag{3.14}$$

The location of the surface is not known, and the free surface boundary condition depends on the mathematical expression below:

$$\phi \wedge f \tag{3.15}$$

The combination of all the boundary conditions into one form of equation gives the mathematical expression below:

$$\frac{\delta f}{\delta t} - \frac{\delta \emptyset}{\delta \zeta} = \ 0 \ \ on \ \ \zeta \ = \ 0 \tag{3.16}$$

$$gf - \frac{\delta \emptyset}{\delta t} = \ 0 \ \ on \ \ \zeta \ = \ 0 \tag{3.17}$$

$$\frac{\delta^2 \phi}{\delta^2 t} - g\frac{\delta \phi}{\delta \zeta} = \ 0 \ \ on \ \ \zeta = 0 \tag{3.18}$$

The solution to the Laplace equation produces a potential solution shown below:

$$k\xi cos(x) + k\eta sin(x) - \omega t \tag{3.19}$$

$$\phi = \frac{gA}{\omega}\frac{\cos \mathrm{h}\, k(h+\zeta)}{coshkh} sin(x) - \omega t \tag{3.20}$$

The acceleration and velocity can be gotten from the expression above, if more expansion of the equation is performed, the boundary conditions must be satisfied by the equation. The modification of the boundary conditions gives the expressions as follow:

Dynamic:

$$\frac{1}{2g}(u^2 + v^2) + z - \frac{1}{g}\frac{\delta \phi}{\delta t} = C(t), z = \eta \tag{3.21}$$

$$\frac{\delta \eta}{\delta t} + u\frac{\delta \eta}{\delta x} = v\ , z\ , \eta \tag{3.22}$$

$$\phi = \frac{g*H}{\omega*2}\frac{\cos \mathrm{h}\, k(h+\zeta)}{coshk(h+\eta)} sin(kx - \ \omega t) \tag{3.23}$$

From this potential function A set of parameters can be found from the potential function aa shown below:

Wavelength: $\lambda = \frac{gT^2}{2\pi}$ (3.24)

Wave number: $K = \frac{2\pi}{\lambda}$ (3.25)

Celerity: $C = \sqrt{\frac{g}{k} tanh\,(kd)}$ (3.26)

Surface elevation: $\eta = \frac{H}{2} cos\theta$ (3.27)

According to Le Mehaute, B., et al, (1980) Stokes in 1847 had the option to discover an answer for waves that were outside the Airy wave hypotheses steepness and relative height impediments. His geometrical extension of the Airy wave has been utilized with acceptable outcomes for waves that are in too shallow waters or are too steep to ever be covered via the Airy hypothesis. His thinking can be rearranged to be, as various sine wave possibilities will consistently fulfil the coherence and base limit conditions equivalent to a solitary potential. The issue is then that there are a few free surface limits. The number of waves is added as potential with a large portion of the period and a large portion of the length of the past request. The following issue is to fulfil two surface limit conditions. [22]. The Stokes approximations are unsatisfactory to portray rushes of little size contrasted with the diameter, as stirs up extensions under these conditions were veering. (Mehaute, *et al*,1980). The stream hypothesis joins similar thinking as the Stokes hypothesis, yet as opposed to tracking down the logical arrangement it takes care of the issue mathematically.

Generally, an expression is given for the Stoke theory as shown below:

$$\psi(x,z) = cz + \sum_n^N X(n)sinh(nk)(z+d)cos\,(nkx) \quad (3.28)$$

If the breaking limit is attained by a wave, it breaks. This scenario can occur in different forms such as plunging, surging, spilling, and collapsing, the occurring types of breaking waves depend on the circumstances surrounding the event. Mathematically,

$$N_1 = \frac{tan\beta}{\sqrt{H/L_0}} \quad (3.29)$$

$$L_0 = gT^2/2\pi \quad (3.30)$$

$\beta - Wave\ steepness$

Spilling $N_I < 0.5$

Plunging $0.5N_I < 3.3$

Collapsing or Surging $N_I > 3.3$

Plunging and spilling are deemed more important than others because they have high tendencies of resulting in high pressures and impulse load pressure. The expectation is that the loads should cover a very little area within a short period.

3.2 Criteria for Breaking Waves

The prediction of wave instability and the eventual breaking of the waves leads to the development of the criteria for breaking of waves, taking the breaking of shallow water and deep water into consideration, the breaker height to the depth ratio is expressed as:

$$\gamma_b = \frac{H_b}{d_b} \tag{3.31}$$

Where γ_b varies between 0.7 and 1.2

In his study, Miche (1944) discovered the overall limiting steepness of waves as

$$\left(\frac{H}{L}\right)_b = 0.14 tanh\ \left(2\pi \frac{d_b}{L_b}\right) \tag{3.32}$$

The increase in depth to deep water results in the limiting steepness to approach 0.14 (1/7) Waves with instability and eventual breaking of the higher steepness. The assumption that the seabed is a flat surface is the only reason that validates this formulation. There is a modification to the criteria if the seabed is sloping which is described below:

$$\frac{H_b}{H_0} = 0.14 tanh\ \left((0.8 + 5S)2\pi \frac{d_b}{L_b}\right) s\ <\ 0.1 \tag{3.33}$$

$$\frac{H_B}{H_0} = 0.14 tanh\ \left((0.13)2\pi \frac{d_b}{L_b}\right) s\ >\ 0.1 \tag{3.34}$$

In shallow waters, the Cnoidal hypothesis offers the best outcomes on wave steepness, however it over gauges the frequency and wave celerity. The Stokes and stream hypothesis will hence be the ones applied in this postulation, as the celerity is significant for the breaking wave load. For deep waters, the breaking point can be thought to be near.

$$\frac{H}{L} = \frac{1}{7} \tag{3.35}$$

The Morrison Equation is a method of assessing the pile because of non-breaking waves on slender piles. It utilizes the wave molecule potential subsidiaries joined with observational elements to get subsequent power from the passing waves. Since both speed increase and speed will cause pressure impulse on the pile, the condition is isolated into two terms. Every one of these records for a piece of the pressure that is applied to the cylinder. The dormancy term in the condition records forces because of the water molecule speed increase, while the drag term represents water molecule speed. This strategy has been utilized to gauge forces that are in acceptable arrangement the real estimated loads (Wienke, and Oumeraci, 2005). The drag coefficient is resolved as a dimensionless capacity of viscosity and Reynolds number.

$$R_e = \frac{u_o D}{v} \tag{3.36}$$

The inertia coefficient is assessed as the force created by the Froude Krylov force though the speed increase of current would cause pressure on the outside of the cylindrical structure. At the point when a cylindrical structure is a little similar to the frequency, this speed increase is thought to be consistent. The liquid around the little cylindrical structure will be hauled along as the liquid passes the cylindrical structure. This extra mass speed increase brings about an increase in the force on the cylindrical structure. The proportion of extra mass concerning the real mass of water influenced is utilized to deliver the mass coefficient that is utilized to scale the inertia term of the Morrison equation.

The Morrison equation is given as follows:

$$F_{total} = F_D + F_I \tag{3.37}$$

$$F_D = \int_{-d}^{\eta} \frac{1}{2} \rho C_d D u(z,\theta) \vee u(z,\theta) \vee dz \tag{3.38}$$

$$F_1 = \int_{-d}^{\eta} \rho\, C_m \pi D^2 u\,(z,\theta) \vee \; dz \tag{3.39}$$

3.3 Slamming Waves

At the point when a wave stage passes a design while breaking or only before breaking, the wave can have a structure that is close to vertical, causing a quick change in pressure as it passes. The brief span and enormous extent of this pressure make it strange to change and execute it into one of the current terms and subsequently it is added in as a different term of the all-out pressure condition. The term is normally alluded to as slamming waves.

$$F_{total} = F_D + F_I + F_s \tag{3.40}$$

For round and hollow areas, it is expected that the water acts like a level surface hitting a level plate. The subsequent impulse pressure was determined utilizing the Bernoulli condition and thinking about the likely stream. These were the presumptions made by Von Karman as the reason for his thought of a wave slamming condition.

Von Karmans formulation

$$F_S = \rho_w R C^2 C_S\,, C_S = \pi\left(1 - \frac{C}{R}t\right), at \;\; t = 0 \;\; => \;\; C_S = \pi \tag{3.41}$$

$$F_S = \rho_w R C^2 \pi \tag{3.42}$$

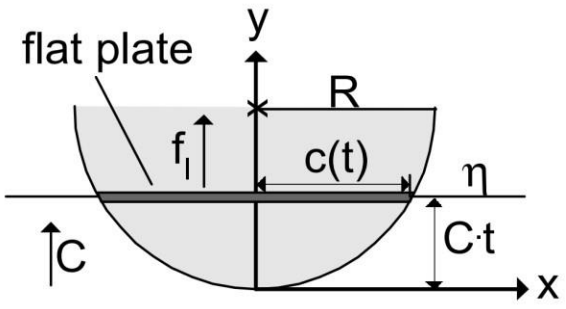

Fig. 3.1 Von Karman's formulation (Wienke, and Oumeraci, 2005)

At the point when a wave moves past a round and hollow cross-segment, the free water surface will misshape. This is the impact that isn't represented in Von Karman's detailing of a slamming occasion. This impact portrayed as pile impact will cause the real slamming occasion to happen somewhat in front of the wave stage. Wagner's formulation changes the definition proposed by Von Karman to represent this impact.

Wagners Formulation

$F_S = \rho_w R C^2 C_s$, at t= 0 => $= 2\pi$ (3.43)

$F_S = 2\rho_w R C^2 \pi$ (3.44)

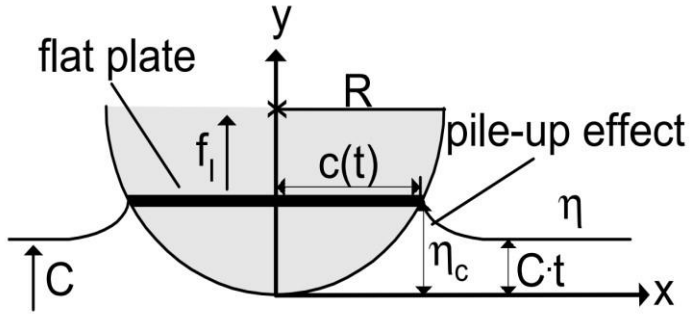

Fig 3.1 Illustration of Wagner's formulation (Wienke, and Oumeraci, 2005)

$$F_S = \rho_w R C^2 C_s \tag{3.45}$$

$$Tdruation_{standards} = \frac{13D}{64c} \tag{3.46}$$

The Von Karman/Wagner formulation just accounted for a unit length of the cylindrical structure, so to discover the complete load, a connection to the size/length of the effect region is required. Goda (1966) utilizes a twisting element to represent the "sway" length, the twisting component is a level of the surface rise at the most noteworthy place of the peak contrasted with Stillwater level. The tendency of the water surface likewise assumes a part in the length and seriousness of the effect. Goda states that an vertical surge of water the tendency and rise time is expected to nothing. A tendency further from vertical and an expansion in ascent season of the maximum effect pressure tends to decrease the slamming force. The rising time is additionally essential since it incredibly influences the dynamic reaction of the design.

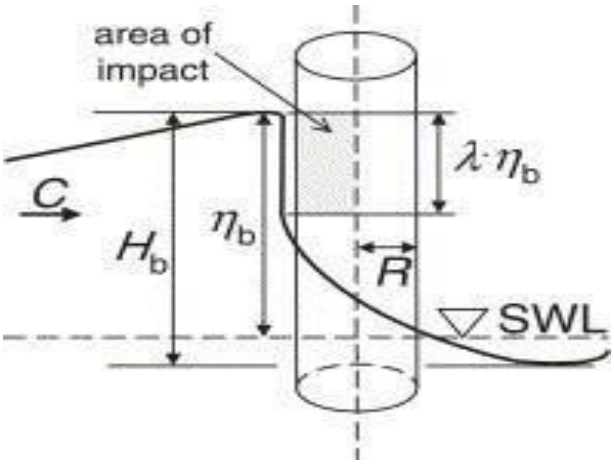

Fig. 3.2 curl effect (Wienke, and Oumeraci, 2005)

The total force of slamming on a cylinder is expressed as

$$F_S = \lambda \eta_b \rho_w R C^2 C_s \tag{3.47}$$

3.4 Description of the Model

In coastal engineering, the impact force on monopiles as a result of breaking waves is mostly determined according to Goda *et al* (1966) as

$$F_1(t) = \lambda.\eta_b . \pi . \rho . R . C^2 \left(1 - \frac{C}{R}T\right) \quad (3.48)$$

Where:

$\lambda.\eta_b$ = the height of the impact area

C = celerity of the wave

η_b = the crest height of the breaking wave

λ = the curling factor

R= radius of the cylinder

ρ = density of the fluid

The assumption applied is that the impact area height $\lambda.\eta_b$ is vertical and moves with wave celerity C. The force impact is distributed along with the height, thus eqn. 8 becomes:

$$F_1(t) = \pi . \rho . R . V^2 \left(1 - \frac{C}{R}t\right) \quad (3.49)$$

Where C = V

Eqn.3.49 shows that the line force is maximum at t =0 at the beginning of the impact and eqn.3.49 becomes

$$F_1 = \pi . \rho . R . V^2 \quad (3.50)$$

Eqn. 10 agrees with von Karman's (1929) on the line of force. However, according to Goda (1966), the higher-order terms for the plate width variation concerning time were used to determine the time history. Most commonly, the slamming coefficient C_s is used for the description of the maximum in-line force per unit height, that is,

$$F_1 = C_s . \rho . R . V^2 \quad (3.51)$$

$C_s = \pi$ according to the Goda *et. al* (1966) model formulation, before then, Wagner (1932)'s solution to peak pressure at the period of the impact of an object on a still fluid had predicted a slamming coefficient of $C_s = 2\pi$ while the method of matched asymptotic expansions was used by Cointe & Armand (1987) to provide a solution to the boundary condition of the surface of flow within the vicinity of the structure and also the velocity potential. A solution of the slamming coefficient $C_s = 2\pi$ was also provided in the model.

The measurement from a site test was taken by Hallowell *et al.* (2016) for the identification of breaking waves and quantifying their impact load variability. The results from the study indicated that the application of the Goda *et al.* (1966) model to calculate the mudline moments was the most consistent model with the measurement taken.

The model of the pressure impulse for slamming wave on a vertical wall is based on the expression:

$$\frac{P}{\rho U H}\left(\frac{x}{H}, \frac{y}{W}, \frac{z}{H}\right) = f\left(\frac{b}{H}, \mu, \frac{W}{H}\right) \quad (3.51)$$

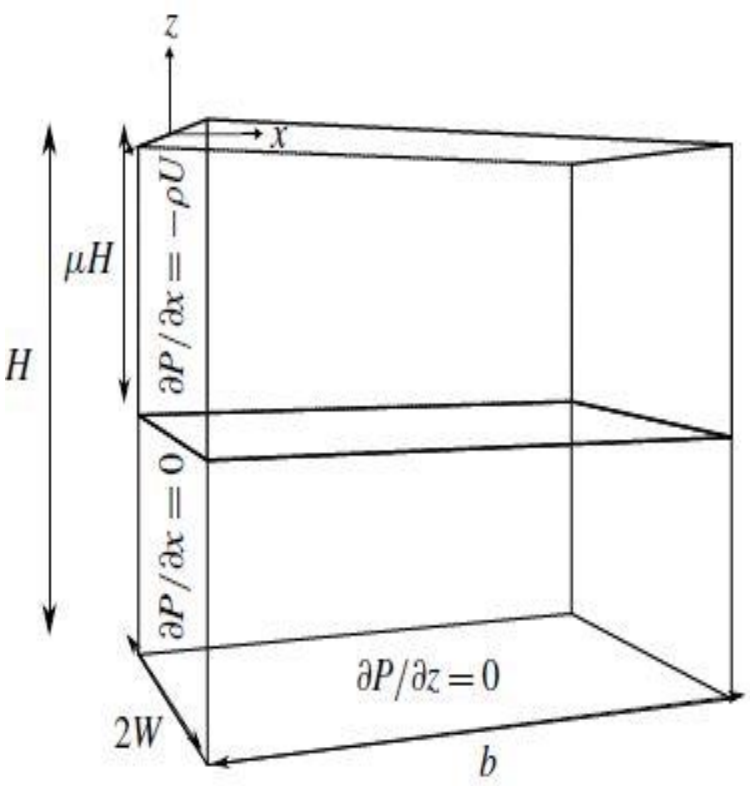

Figure 3.3: Definition sketch for 3D block impact on a vertical wall (Ghadrian and Bredmose, 2019)

Where $\frac{b}{H}$ represent the relative length of the block

$\frac{W}{H}$ represents the relative width of the block

μ represent the relative height of the impacting zone

The vertical wall is situated at x=0, during sway, the vertical was affected by liquid at a typical speed U limited inside - μH ≤ z ≤ 0. Where μ addresses the proportion of affecting liquid height to the height of the entire liquid. With the comprehension from the 3D box influence issue, it is kept on being affected on the round and hollow construction. First, the essential example of an

axisymmetric influence is inspected. A wavefront hits the tube-shaped construction from all headings with a commonplace speed of U in the vertical zone −μH 6 z 6 0. Underneath this zone, in −H 6 z 6 −μH, the fluid contacts the tube-shaped construction at influence. The outside scope of the influencing fluid is implied by b, and the round and hollow construction clear by a. The Laplace condition is gotten comfortable the cylinder molded work with the system to yield:

$$P = \sum_{m=1}^{\infty}\sum_{n=1}^{\infty}\left(A_{mn}cos\ \left(\frac{L_m\theta}{\theta_{max}}\right)sin\left(K_n\frac{z}{H}\right)\frac{I_{qm}\left(K_n\frac{r}{H}\right)+\alpha_{mn}K_{qm}\left(K_n\frac{r}{H}\right)}{\partial_r\left(I_{qm}\left(K_n\frac{r}{H}\right)+\alpha_{mn}K_{qm}\left(K_n\frac{r}{H}\right)\right)_{r=\alpha}}\right) \quad (3.52)$$

where kn = (n − 1/2)π, ∂r is the partial derivative with regards to r, I0 and K0 are the first and second kind modified Bessel functions of zeroth order.

$$\alpha_{mn} = \frac{-I_{qm}\left(K_n\frac{b}{H}\right)}{K_{qm}\left(K_n\frac{b}{H}\right)} \quad (3.53)$$

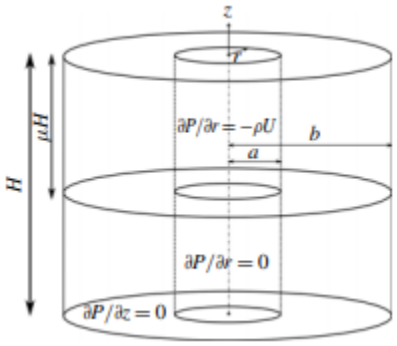

Fig. 3.4 axisymmetric impact on a vertical cylinder (Ghadrian and Bredmose, 2019)

The changed Bessel functions were picked for the spiral reliance due to their non-oscillatory change which is appropriate for the impact issue. A direct blend of the two functions is utilized here to guarantee consistency with the limit condition. From equation 3.48 the non-dimensional

pressure impulse on the cylindrical structure relies upon the overall external radius of the affecting liquid b/H, the total height of the fluid μ, and the proportion of the inward to external radius a/b:

$$\frac{P}{\rho UH}\left(\frac{r}{H},\frac{z}{H}\right)=f\left(\frac{b}{H},\mu,\frac{\alpha}{b}\right) \tag{3.54}$$

For an impact of an idealized wave on a cylinder with an azimuth limit,

$$P=\sum_{m=1}^{\infty}\sum_{n=1}^{\infty}\left(A_{mn}cos\ \left(\frac{L_m\theta}{\theta_{max}}\right)sin\left(K_n\frac{z}{H}\right)\frac{I_{qm}\left(K_n\frac{r}{H}\right)+\alpha_{mn}K_{qm}\left(K_n\frac{r}{H}\right)}{\partial_r\left(I_{qm}\left(K_n\frac{r}{H}\right)+\alpha_{mn}K_{qm}\left(K_n\frac{r}{H}\right)\right)_{r=\alpha}}\right) \tag{3.55}$$

where Lm = (m − 1/2)π, kn = (n − 1/2)π and qm = Lm/θmax is the order of the Bessel functions. Further αmn is chosen such that P = 0 at r = b

$$\alpha_{mn}=\frac{-I_{qm}\left(K_n\frac{b}{H}\right)}{K_{qm}\left(K_n\frac{b}{H}\right)} \tag{3.56}$$

And,

$$A_{mn}=\frac{2\rho U}{\theta_{max}}\ \frac{1-cos(K_n\mu)}{K_n}\ \int_{-\theta_{max}}^{\theta_{max}}cos(\theta)cos\left(\frac{L_m\theta}{\theta_{max}}\right)d\theta\ dz \tag{3.57}$$

$$\frac{P}{\rho UH}\left(\frac{r}{H},\theta,\frac{z}{H}\right)=f\left(\frac{b}{H},\mu,\frac{a}{b},\theta_{max}\right) \tag{3.58}$$

4. RESULT AND ANALYSIS

The analysis obtained are introduced in this section. The problem which was addressed mathematically was executed in MATLAB as a m-file in the form of an equation alongside the boundary conditions until the solution converges and all boundary conditions were satisfied. The model utilized MATLAB to reproduce the outcome gotten by Ghadrian and Bredmose (2019). The outcome obtained show a brilliant understanding between the previous studies. A parametric report was done to observe the impact of the parameter of interest and how the cylindrical structure behaves. Mathematical techniques are additionally usually used to get the best mathematical guess to tackle the wave-structure problem. The fundamental reason for mathematical demonstrating is to comprehend the actual issue and show it in a typical numerical construction (Tonti, 1975). The mathematical cycle incorporates a standard advance where the issue is characterized, demonstrated numerically and solved using mathematical software. There are things to consider while choosing the most appropriate mathematical techniques to be used in solving the problem which are the accuracy, required computational limit and performance. The outcome of the computational model relies upon the numerical problems, which considers the administering conditions and limit conditions. The primary distinction between these strategies is discretisation.

The most recent approaches utilized is the Finite Difference Method (FDM) (Liszka and Orkisz, 1980). Basically, this methodology utilizes a topologically square while discretising the actual space. The primary drawback of this technique is that it faces difficulties when settling a more complex calculation because of the trouble of demonstrating an unstructured lattice (LeVeque, 2005). The Finite Element Method and the Finite Volume Method were subsequently used to solve these difficulties, both these strategies can be portrayed as the basic type of the answer for the Partial Differential Equation (PDE), and when duplicated with the weighted capacity, the given

condition is debilitated. One of the fundamental benefits of the FEM is the adaptability which permits muddled calculations to be demonstrated numerically, i.e., the utilization of non-uniform matrices, and discretization size which permits higher request time discretization issues to be tackled, like considering the nonlinearity of waves. The limit component technique (BEM) (Hanna and Humar, 1982; Becker, 1992) gives the arrangement by changing the area given differential conditions into vital characters outside the limit. The FEM and FVM techniques are very comparable. The FVM, which utilizes cell volumes as opposed to hubs during discretization, has been utilized to effectively demonstrate wave diffraction around cylinders (Laghrouche *et al.*). FVM requires less computational memory and force contrasted with the FEM. This is additionally influenced by the way that the FVM stores the reliant qualities in the focal point of the limited volume while the FEM stores the reliant qualities at the component hubs. The strategy for discretisation additionally varies, FVM discretisation is by tackling the indispensable type of the halfway differential condition, while the FEM utilizes explicit shape capacity to discretise the space. The arrangement of the FVM is discrete while the arrangement of the FEM is nonstop. As far as programming, the FVM is simpler contrasted with the FEM. The different mathematical strategies accessible can be coupled together to stretch out their capacity to tackle for additional designing issues. For instance, the FEM and BEM can be coupled to address the fluid and design issue in the time area and for wave reproduction at higher Reynolds number (Young et al., 2001). The FEM is normally used to address the nonlinear contributor to the issue and the BEM is utilized to handle the issue of an emanated wave, which proliferates to limitlessness. Designs set in the sea have a limit state of radiation to vastness to be fulfilled, bringing about an unbounded area. Rather than defining a surmised limit at the most distant finish of the construction, the FEM can be combined with different techniques, where the close to handle utilizes the FEM to handle the

nonlinearity while the far field utilizes different strategies to determine the issue in the unbounded area. FEM can be combined with various strategies (Zienkiewicz et al., 2014). One of the significant difficulties for the FEM is to acquire arrangements fulfilling the emanated limit condition. The technique to defeat the unpredictable recurrence that frequently happens while applying BEM to wave diffraction issues has been tended to (Lee and Sclavounos, 1989), while BEM can likewise be combined with other existing mathematical strategies.

The Fluid Impulse Theory (FIT) is a minimized, quick yet generally precise model to recreate the nonlinear wave loads on offshore constructions. It is a rearranged scientific model contrasted with the weighty computational-cost Computational Fluid Dynamics (CFD) models, a CFD model generally requires days to figure the single-recurrence wave sway for 10-second arrangement while by utilizing FIT, the full-range (with many frequencies) wave sway for 100-second arrangement requires a few minutes. So FIT can be effortlessly applied in the starter configuration cycle of slim round and hollow offshore designs, similar to base fixed offshore wind turbines, coat stages or stage risers. Furthermore, it can likewise be utilized as a quick computational instrument to get the factual properties of offshore constructions to help anticipate the limit loading. The study reproduced validated the model against an actual wave impact. The wave selected is basically focused on phase and direction for a sea state of Hs = 9.5 m and Tp = 12 s in 33 m water diameter with a cylinder width of 7 m. Computational fluid elements results at scale 1 : 50 for this effect were introduced by Ghadirian *et al.* (2016). The affecting water spreads to the sides, facing up and downwards in the wake of affecting the monopile. Here b is picked as the separation from the cylinder community to the rear of the wave peak at the still-water level. Further μ is resolved from the height of the breaker. Thusly b/H = 0.64, μ = 0.12 and a/b = 0.13, with θmax left as the solitary free boundary. The inline pressure time arrangement from the CFD model is introduced. As a vital

advance to disengage the effect power motivation from the commitment prompted by the non-affecting pieces of the wave, the tension on the cylinder from not long before the effect was deducted from constantly moments in the CFD results. At that point the time necessary from the start of the effect until the end was determined. The biggest pressure impulse is seen beneath z/H = −0.05 at θ/θmax = 0 and the pressure impulse stretches out down to z/H = −0.2. Note that, regardless of the deduction of the pressure impulse not long before sway, a portion of the all-inclusive motivation might be brought about by the kinematics of the actual wave and not really the pummelling sway. It is seen that the pressure impulse diminishes to around zero at near θmax, which shows that the picked azimuthal breaking point is reasonable. The worth of θmax was picked to such an extent that the effect power motivation of the CFD model was equivalent to the wall coordinated pressure impulse in the inline course. This prompted θmax = π/4 with just 3 % over prediction of the incautious pressure by the model. An overall decent consistency between the model and CFD pressure motivation appropriation and greatness is noticed. The pressure impulse is confined in the upper layer in both the CFD and model outcomes, which is connected to the little breaker height proportion. The model outcome depends on an attack of θmax to coordinate with the pressure impulse.

For a vertical cylinder, the model was validated against existing literature with μ = 0.5, $\frac{b}{H}$ = 1, and $\frac{W}{H}$ =0.5 by Ghadrian & Bredmose (2019) while the present result employed MATLAB to reproduce the results obtained with same parameters. The results gotten from MATLAB as shown are in excellent agreement. The present study reproduced the result obtained by Ghadrian & Bredmose (2019).

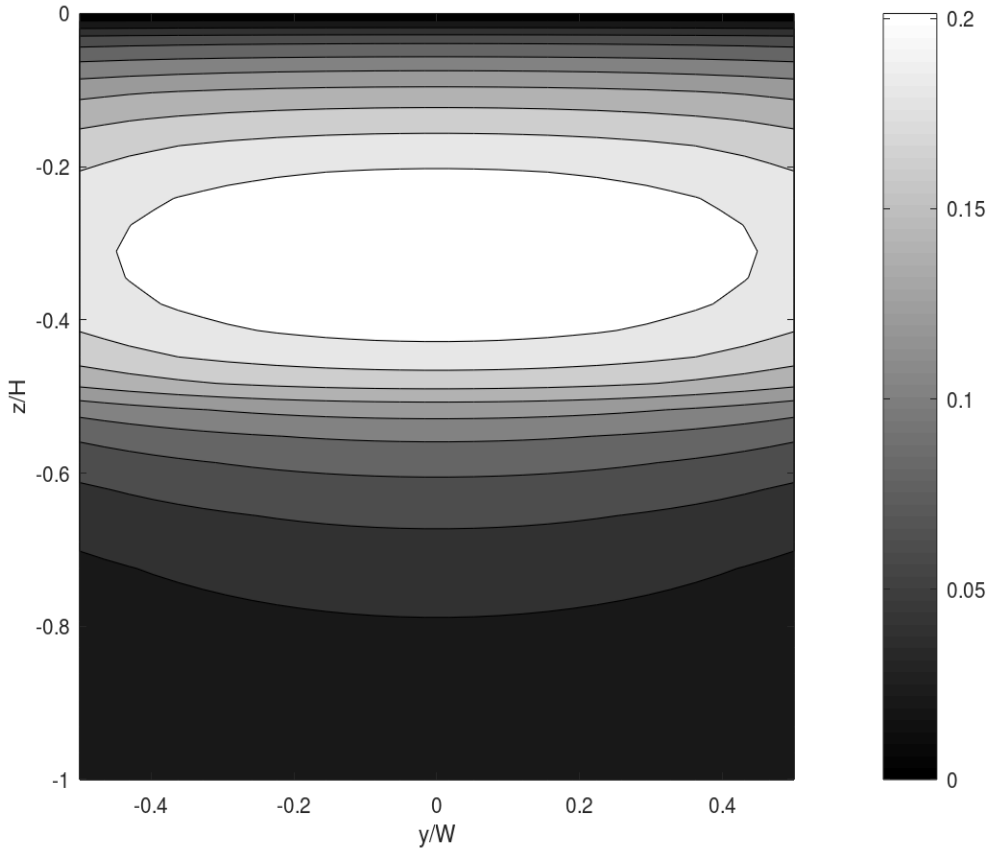

Figure 4.1: Pressure impulse of a finite-width fluid block on a flat vertical plate at μ = 0.5, $\frac{b}{H}$ = 1, and $\frac{W}{H}$ =0.5

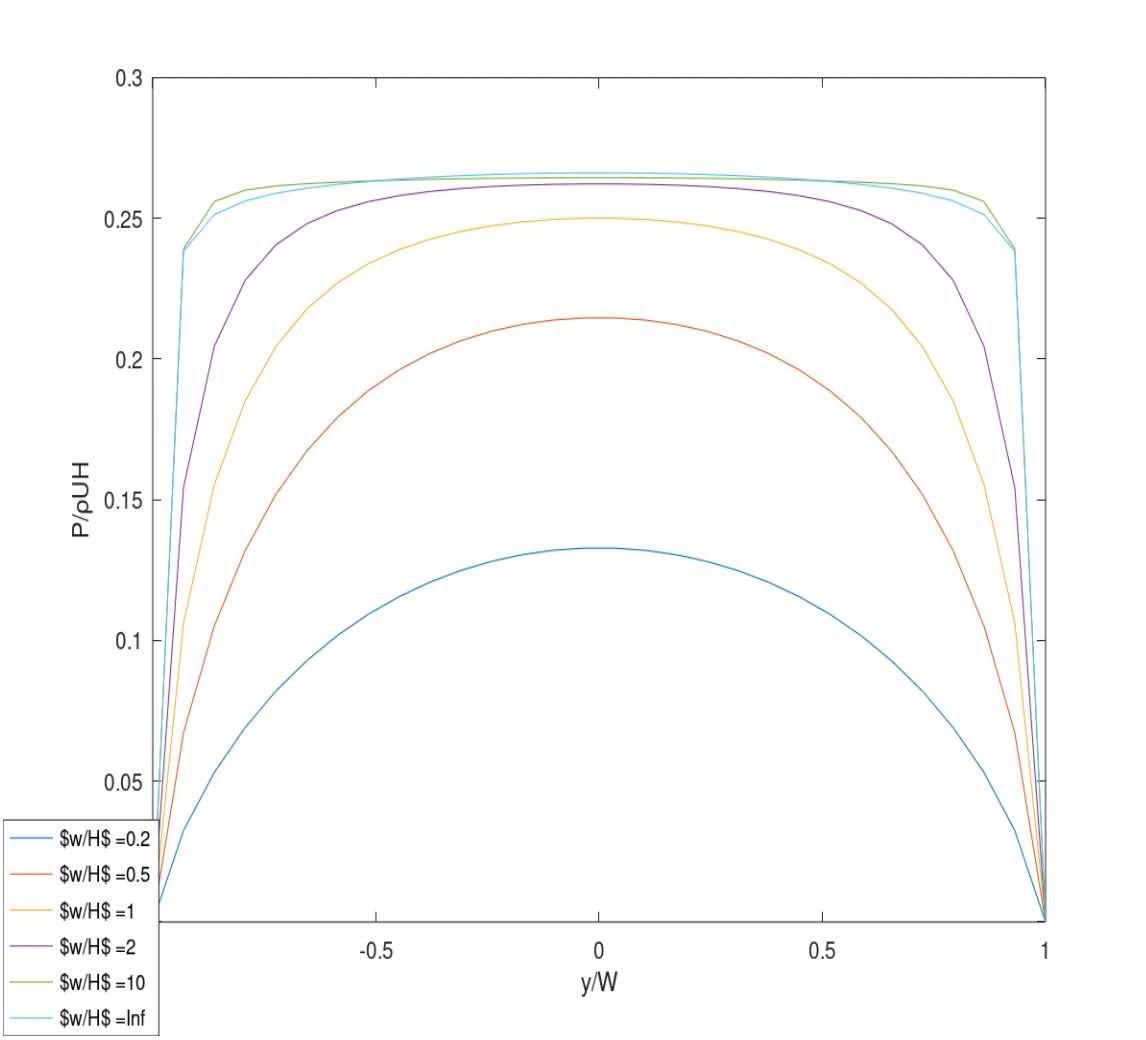

Figure 4.2: Pressure impulse as a function of width of the impacting block, plotted at the mid-height on the flat wall at z/H = -μ/2 and x/H = 0

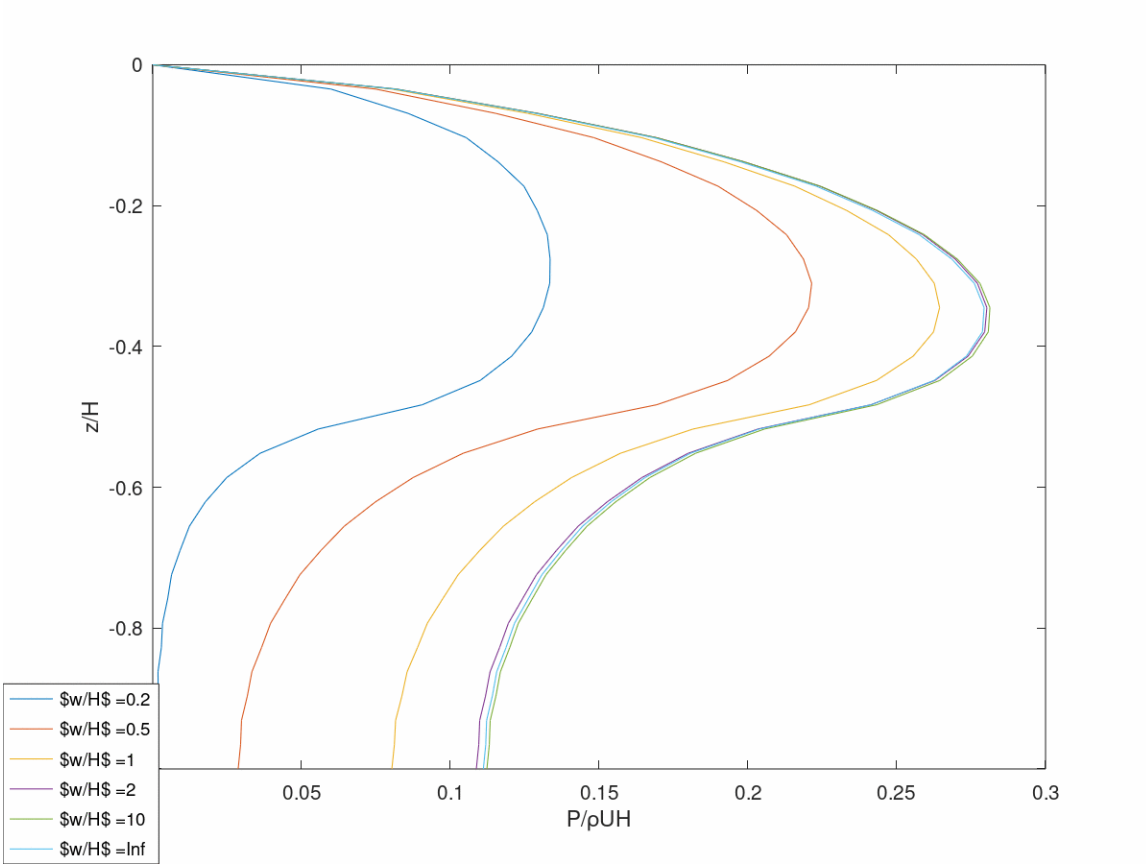

Figure 4.3: Pressure impulse as a function of width of the impacting block, plotted at the mid-width on the flat wall at y/W =0, x/H =0

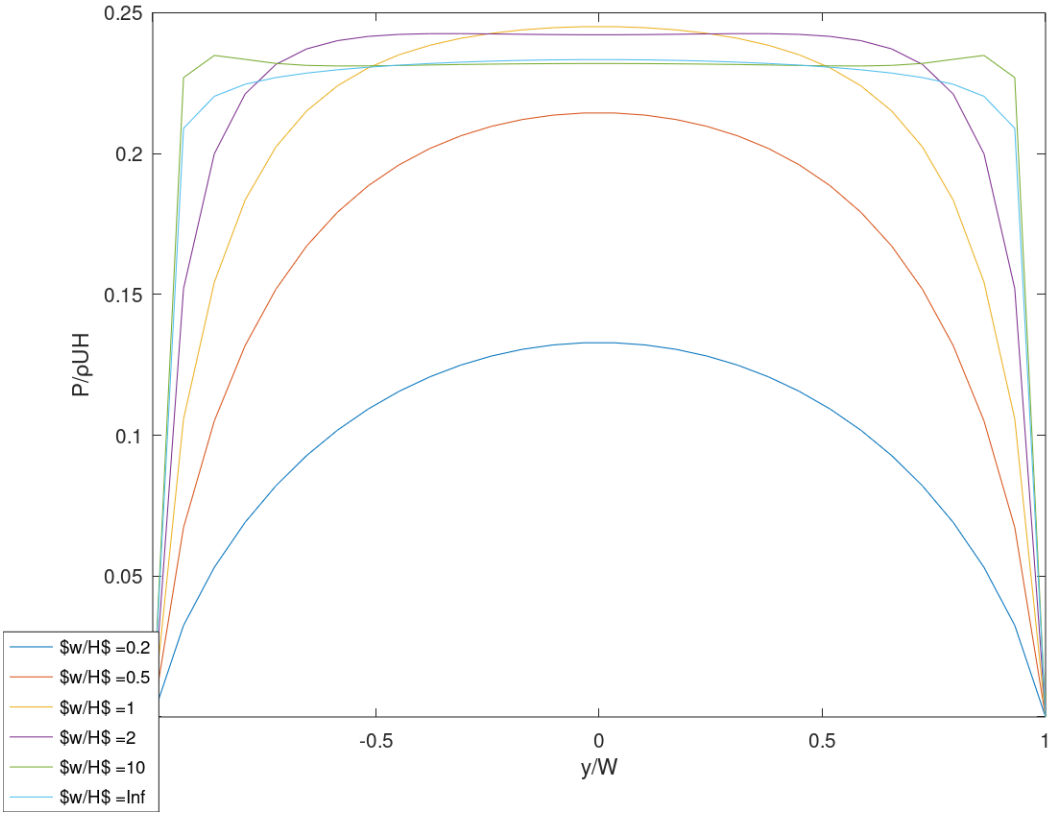

Figure 4.4: Pressure impulse as a function of width of the impacting block, plotted at the mid-height on the flat wall at z/H = -μ/2 and x/H = 0

The equations for the vertical cylinder is decreased to the two-dimensional 2D arrangement of Cooker and Peregrine (1995) as W→ ∞ and furthermore, eqn. 4.3 relies upon the second horizontal direction and the hyperbolic function coefficients. It is noticed that the normal pressure impulse depends on eqn. 4.2. The outcome in fig. 4.3 demonstrates that there is an augmentation of the impulse pressure at the focal point of the square to the lower part of the height more than - μH, the ramifications of this is that the liquid at the base conveys some piece of the pressure impulse. As seen in fig.4.3, the pressure impulse relies upon the width of the structure. The outcome shows that there is a most extreme pressure impulse at the plate area, i.e., at y/W = 0 with an increase in equivalent proportionate with the width until it arrives at the two-dimensional 2D breaking point

addressed on the figure by a strong line. The outcome is acquired for W/H ≈ 2 at the focal point of the plate and along the edge of the wall for a bigger upsides of W/H. As demonstrated in fig.4.4, the diagram for the pressure impulse at the plate vertical centreline is plotted regarding the height of the square. It is demonstrated that the impact of the square effect watches out for a two-dimensional 2D case as the width of the square liquid increases to W/H = 10. Some new parameters of interest were varied and some other results were obtained: The dependence on the width of the impacting block fluid $\frac{W}{H}$ are shown for μ=0.5 and $\frac{W}{H}$ = 1 and also, the Pressure impulse as a function of width of the impacting block, plotted at the mid-width on the flat wall at y/W =0, x/H =0 was plotted at the mid-width on the flat wall at y/W =0, x/H =0.

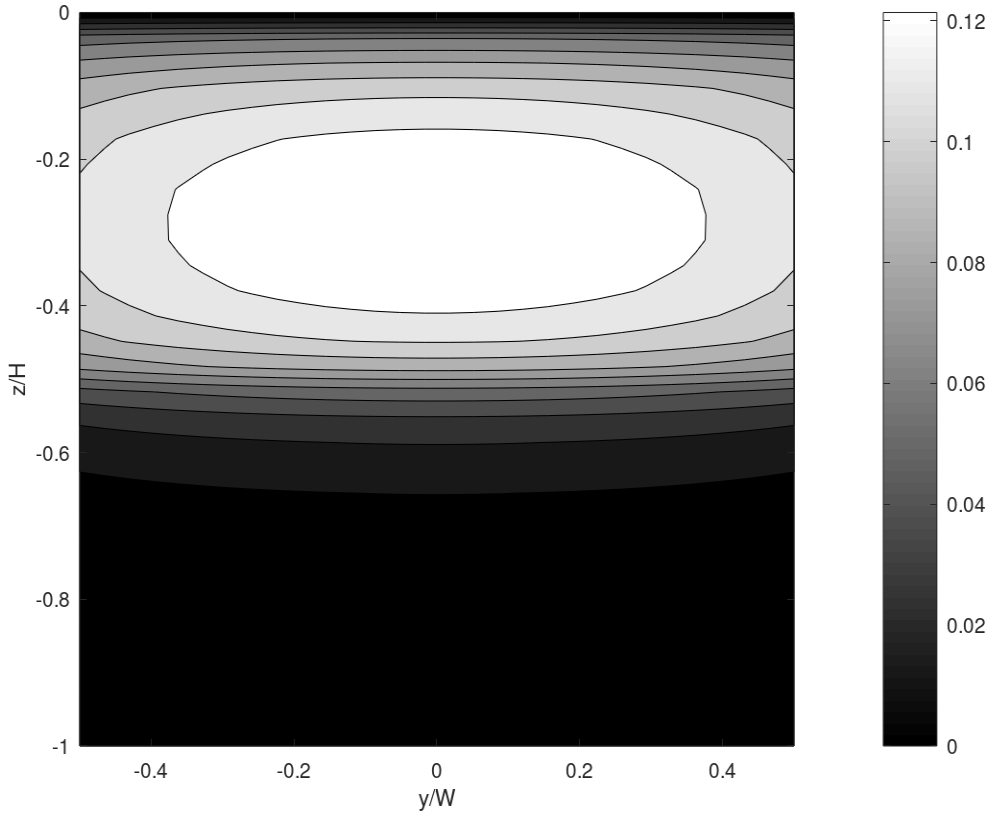

Figure 4.5: Pressure impulse of a finite-width fluid block on a flat vertical plate at $\frac{W}{H}$ =0.2

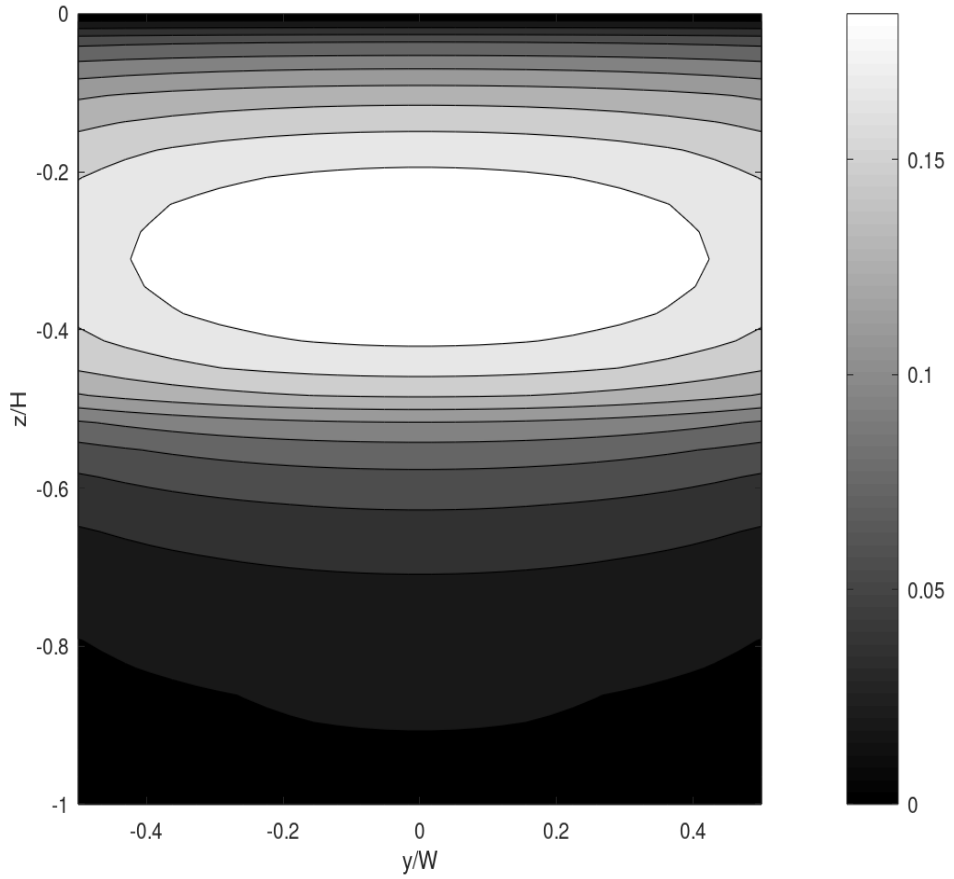

Figure 4.6: Pressure impulse of a finite-width fluid block on a flat vertical plate at $\frac{W}{H}$ =0.4

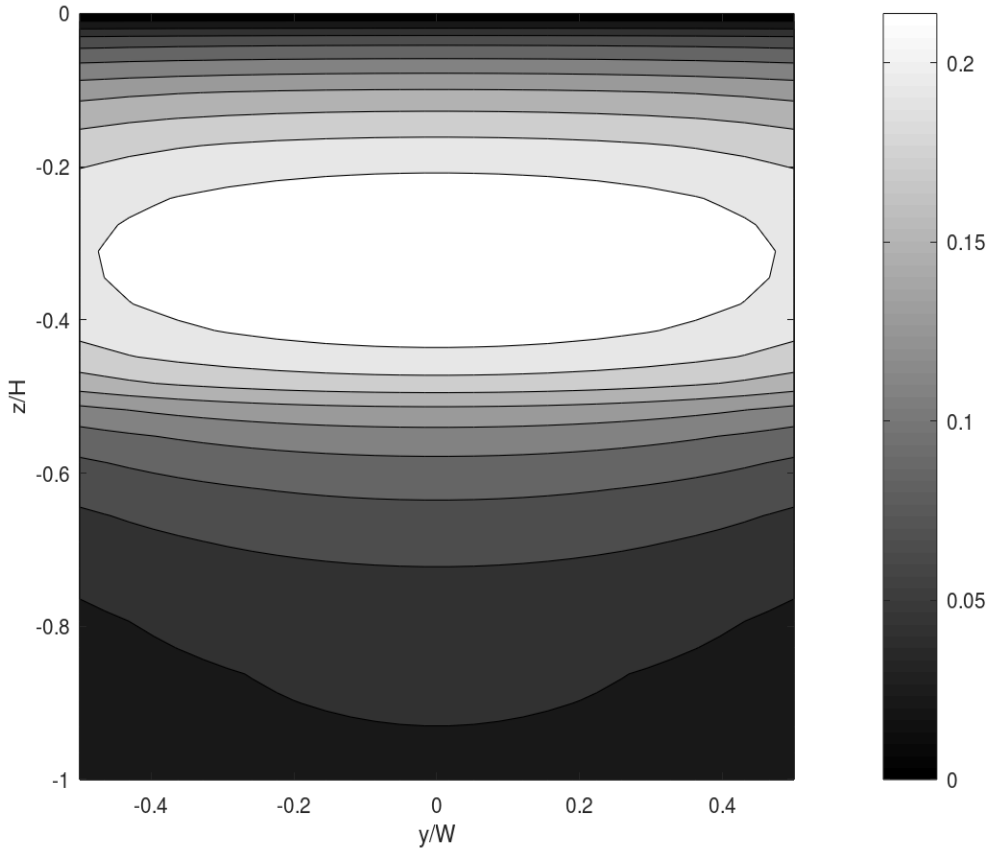

Figure 4.7: Pressure impulse of a finite-width fluid block on a flat vertical plate at $\frac{W}{H}$ =0.4

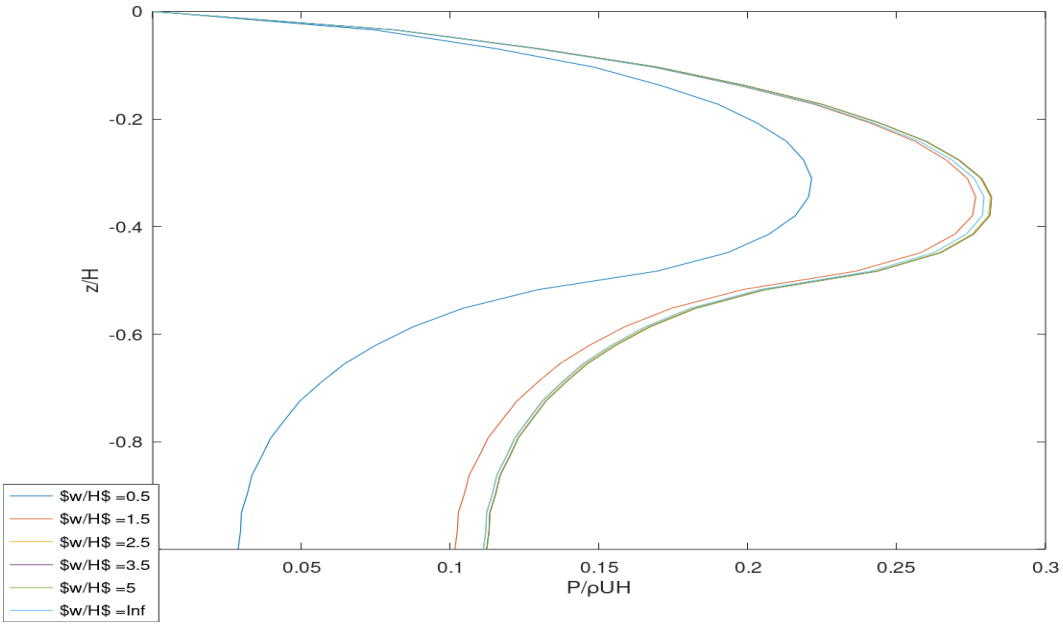

Fig. 4.8: Pressure impulse as a function of width of the impacting block, plotted at the mid-width on the flat wall at y/W =0, x/H =0

The acting force increases as the azimuthal point limit increases up until π/2 where it reaches its peak. The complete pressure impulse of the model can measure up to the current effect models of Goda et al. (1966) and Wienke and Oumeraci (2005). The pressure impulse is determined dependent on these models has roughly 190 % and 100 % above-prediction individually. The above prediction might be brought about by the anticipated most extreme force just as the time frame, which has been approved less significantly in past studies. The results reproduced as obtained are illustrated and discussed as shown below:

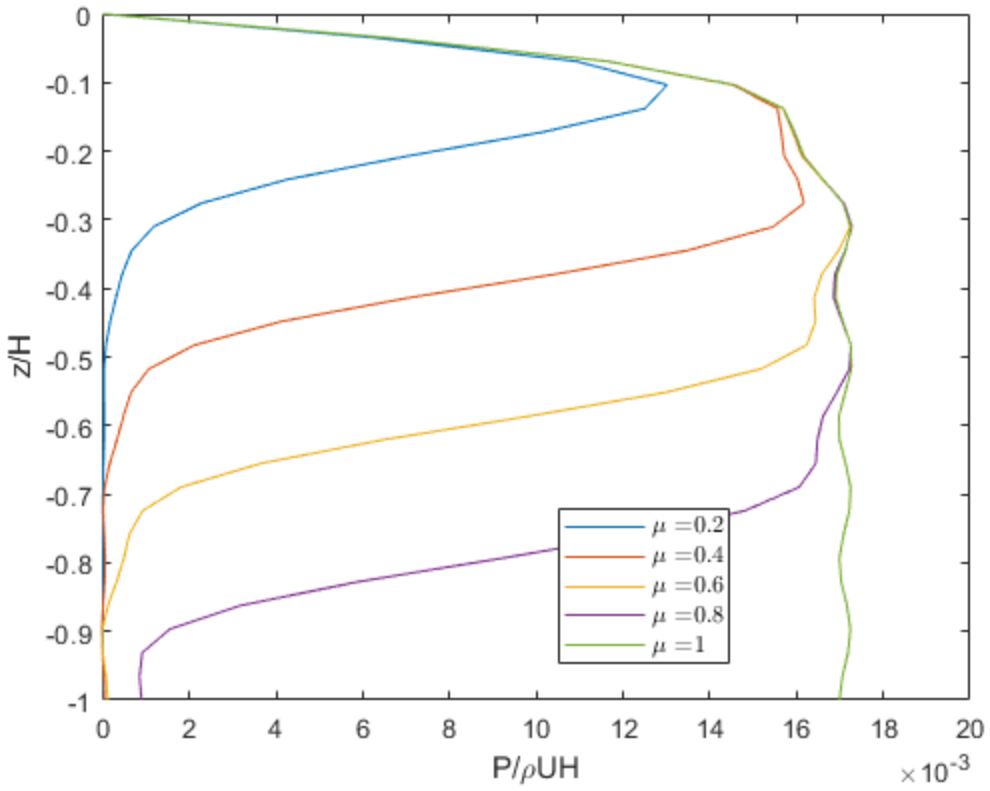

Fig. 4.9: Dimensionless pressure impulse on the inner cylinder, at θ = 0, plotted as a function of z/H for several values of μ.

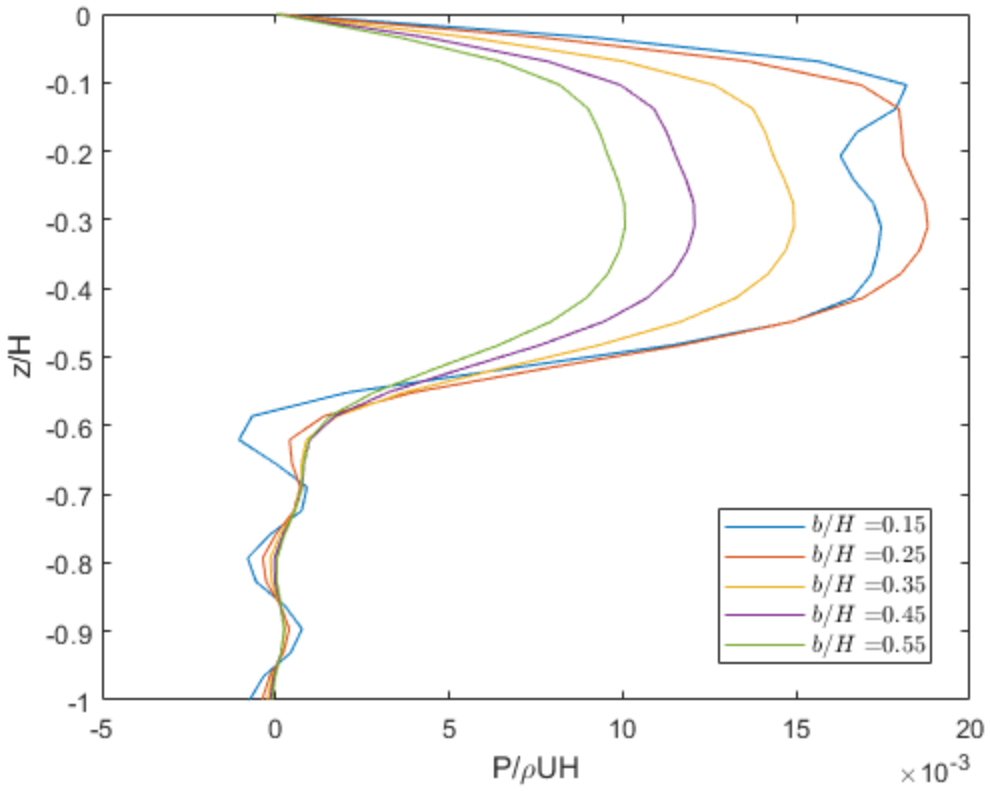

Fig 4.10: Dimensionless pressure impulse on the inner cylinder, at θ = 0, plotted as a function of z/H, (a) for several values of b/H

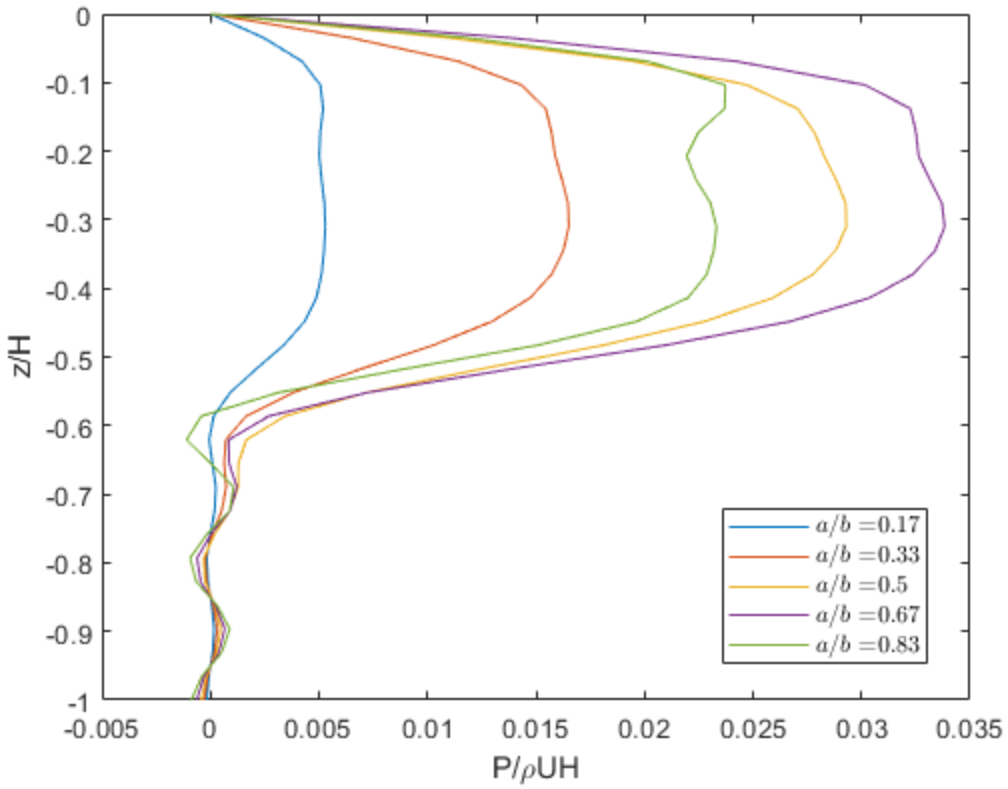

Fig 4.11: Dimensionless pressure impulse on the inner cylinder plotted (a) as a function of z/H, at θ = 0, for several values of a/b.

The reliance on the general length of the affecting wave b/H as appeared in figure 4.10 for θ = 0, μ = 0.5, a/H = 0.1 and θmax = π/4. As b/H increases up to 0.35, the pressure impulse increases in all dimensions and afterward stays unaltered. This shows an asymptotic conduct for expanding b/H as shown. A similar asymptotic conduct was seen by Cooker and Peregrine (1995) for the 2D level plate case. The reliance on the height of the impact area is also examined as shown in figure 4.10. A width of b/H = 0.3 is utilized and μ, θmax and a/H are indistinguishable from what is obtainable in figure 4.9. By the expansion of μ, the tilt of the pressure impulse as expected drops down and results to the expansion of the pressure impulse. The outcomes from this figure are likewise steady with the ones appeared in Cooker and Peregrine (1995). The varying parameters

as for the relative inward span a/b is examined in figure 4.11 for $\mu = 0.5$, $\theta max = \pi/4$ and $b/H = 0.3$. The pressure impulse increases as a/b increases up to $a/b = 0.5$. For a/b higher than 0.67, the pressure impulse diminishes also to the case appeared for the axisymmetric sway. To begin with, the region on the cylindrical structure that ingests episode force increases as the radius increases. Thereby the pressure impulse increases. Nonetheless, simultaneously the volume of fluid influence on the cylindrical structure diminishes, so inside the stretch $0.5 < a/b < 0.7$, a worth of a/b happens for which the appropriation has a general greatest in pressure impulse. This expansion can be clarified by the increase in the absolute affecting volume of liquid $V = (b^2 - a^2)\theta max \mu H$ as θmax increases which is similar to the pressure impulse of the 3D effect of the liquid on the level vertical plate. The pace of increase of the pressure impulse turns out to be continuously more modest as the azimuthal point limit increases until it arrives at its peak at $\theta max = \pi/2$.

5. **DISCUSSION**

The results obtained indicated that there is an increase in the pressure impulse together with the crest length right till the asymptotic boundary, this shows that the model is an effective one for a real impact of wave. Also, it is obtained that the inner radius increases with the pressure impulse till a limit as a result of the cylinder wall that has considerably increased. Meanwhile, the effect of the diminishing incident momentum causes the pressure impulse to decrease as the slamming fluid volume reduces. As shown, the results obtained in this study with MATLAB shows an excellent agreement with the CFD results by Ghadrian & Bredmose (2019) and consistent with Cooker & Peregrine (1995). Future work may validate more loads impacts events against other CFD results so as to gain broad insight and knowledge for accurate prediction of the impulse pressure model.

6. **CONCLUSION**

The breaking wave loads for an idealized wave on a cylinder with azimuth limits with relative length and impact height has been determined in this project using the Pressure Impulse Method. A simplified MATLAB model was developed to calculate the pressure impulse by varying some parameters of interest. The results obtained in this study with MATLAB shows an excellent agreement with the CFD results by Ghadrian & Bredmose (2019) and consistent with Cooker & Peregrine (1995). The analysis of the results obtained presents an accurate solution with respect to the varied parameters and provided an excellent prediction of Ultimate Limit State (ULS) Wave Loads on Bottom Fixed Wind Turbine. In future work, changes dependent on the boundary utilized in the present study can be examined for comparable cases and future work may validate more loads impacts events against other CFD results so as to gain broad insight and knowledge for accurate prediction of the impulse pressure model.

REFERENCES

Bredmose, H., Mariegaard, J., Paulsen, B. T., Jensen, B., Schløer, S., Larsen, T., Kim, T., and Hansen, A. M. (2016). DeRisk— accurate prediction of ULS wave loads. Outlook and

first results. *Energy Procedia*, 94: 379 – 387.

Bredmose, H., Mariegaard, J., Paulsen, B. T., Jensen, B., Schløer, S., Larsen, T., Kim, T., and Hansen, A. M., (2013). The Wave Loads project. Tech. rep., DTU Wind Energy.

Choi, S.J., (2014). Breaking Wave Impact Forces on an Offshore Structure, PhD thesis (UiS No.231). University of Stavanger, Norway, at the Department of Mechanical and

Structural Engineering and Material Science.

Cointe, R. & Armand, J.-L. (1987). Hydrodynamic impact analysis of a cylinder. *Trans ASME J. Offshore Mech. Arctic Engng* 109 (3), 237–243.

Cooker, M. J. & Peregrine, H. (1995). Pressure-Impulse Theory for Liquid Impact Problems. *J. Fluid Mech.* 297, 193–214.

Chella, A.M., Bihs, H., Myrhaug, D., Muskulus, M., (2016). Breaking solitary waves and breaking wave forces on a vertically mounted slender cylinder over an impermeable sloping seabed. *J. Ocean Eng. Mar. Energy*, 1–19.

Chella, A.M., Bihs, H., Myrhaug, D., Muskulus, M. (2015), Breaking characteristics and geometric properties of spilling breakers over slopes, *Coastal Engineering*, 95, 4-19.

Dean, R.G. and R.A. Dalrymple, Coastal processes with engineering applications. 2002, Cambridge, UK : New York: Cambridge, UK : New York: Cambridge University Press.

Fox, R.W., A.T. McDonald, and P.J. Pritchard, Introduction to fluid mechanics. 6th ed. ed. 2004, Hoboken, N.J: Wiley.

Ghadirian, A., Bredmose, H. & Dixen, M. (2016). Breaking Phase Focused Wave Group Loads on Offshore Wind Turbine Monopiles. *J. Phys.: Conf. Ser.* 753 (9).

Ghadirian, A. and H. Bredmose (2019). Pressure impulse theory for a slamming wave on a vertical circular cylinder. *Journal of Fluid Mechanics.* 867.

Goda, Y., Haranaka, S. & Kitahata, M. (1966). Study On Impulsive Breaking Wave Forces on Piles. Tech. Rep.

Hallowell, S., Myers, A. T. & Arwade, S. R. (2016). Variability of breaking wave characteristics and impact loads on offshore wind turbines supported by monopiles. *Wind Energy* 19, 301–312.

Hull, P., Müller, G., (2002). An investigation of breaker heights, shapes and pressures. *Ocean Eng*. 29 (1), 59–79.

Hudspeth, R.T., Waves and wave forces on coastal and ocean structures. 2006, World Scientific: Hackensack, N.J

Leite O.B, (2015). "Review of Design Procedures for Monopile Offshore Wind Structres," University of Porto, Porto.

Marintek, USFOS Geetting Started Strcutural Engineering SINTEF GROUP. 28. Patel, M.H., Dynamics of offshore structures. 1989, London: Butterworths

Lee, K.H., Park, J.H., Baek, D.J., Cho, S., Kim, D.S., (2011). Discussion on optimal shape for wave power converter using oscillating water column. *J. Korean Soc. Coast. Ocean Eng.* 23 (5), 345–357.

Lewandowski, E.M., The dynamics of marine craft: maneuvering and seakeeping. 2004, World Scientific Pub.: Singapore.

Lynn, P.A., Onshore and offshore wind energy : an introduction. 2012, Wiley: Chichester.

Nielsen, P., Coastal and estuarine processes. Advanced series on ocean engineering. Vol. vol. 29. 2009, New Jersey: World Scientific.

Oggiano, L., Pierella, F., Vaal, J. D., Nygaard, T. A., Stenbro, R., and Arens, E., (2017). "Modeling of 2D Irregular Waves on a Sloped Bottom Using a Fully Nonlinear Navier-Stokes / VOF Formulation". *In Proceedings of the International Offshore and Polar Engineering Conference*, pp. 622–629.

Paulsen, B.T., (2013). Efficient Computations of Wave Loads on Offshore Structures, (PhD thesis). Technical University of Denmark, at the Department of Mechanical Engineering.

Rogers, N., (1998). Structural dynamics of offshore wind turbines subject to extreme wave loading. *Proc. of the 20th BWEA Annual Conf.*

Jen-Men Lo, R.G.D., Evaluation of a modified stretched linear wave theory. Proceedings of 20th Conference on Coastal Engineering, 1986.

Ridder, E.J., Aalberts, P., Berg, J., Buchner, B. & Peeringa, J. (2011). The dynamic response of an offshore wind turbine with realistic flexibility to breaking wave impact. *Proc. of the ASME 2011 30th Int. Conf. on Ocean, Offshore and Arctic Eng.*, Rotterdam, The Netherlands.

Wienke, J. & Oumeraci, H. (2005). Breaking wave impact force on a vertical and inclined slender pile – Theoretical and large-scale model investigations. *Coast. Engng* 52 (5), 435–462.

Whitham, G.B., Linear and nonlinear waves. Pure and applied mathematics (Wiley). 1974, New York: Wiley

Wood, D. J. & Peregrine, D. H. (1998). Two and three-dimensional pressure-impulse models of wave impact on structures. *Coast. Engng* 1–3, 1502–1515.

APPENDIX

```
function [Pxyz, P] = PressureImpulseFunction(thetamin, thetamax,zHmin,zHmax,...
                    mu, aoverb, aoverH, rHmin, rHmax, boverH, M, N, Npoints)


%%
rhoUH =1;  % one because you intend to evaluate P/rhoUH
mlarge = M;
nlarge = N;



zoverH =  linspace(zHmin,zHmax, Npoints)';      % limits for z/H
theta = linspace(thetamin, thetamax, Npoints)';  % limits for y/W
roverH = linspace(rHmin, rHmax, Npoints)';     % limits for x/H


% Initializes P(x,y,z)
Pxyz = zeros(size(theta));
```

```
syms roverH_ theta_


for m = 1: mlarge
    for n= 1: nlarge
        L_m = (m - 1/2)*pi ;
        k_n  = (n - 1/2)*pi ;
        qm = L_m/thetamax ;


        % Equation 2.13
        DZ = diff(zoverH,1);
        dz = DZ(1);
        A_mn = 2*rhoUH./thetamax* (1 - cos(k_n *mu))/k_n * ...
            (integral(cos(theta_).*cos(L_m.*theta_./thetamax), [-thetamax, thetamax]))*dz ;


 %                      (double(vpaintegral(cos(theta_).*cos(L_m.*theta_./theta_max),  [-theta_max
theta_max])))*dz ;



        % Equation 2.12
```

```
        alpha_mn = - besseli(qm,k_n.*boverH)./besselk(qm, k_n.*boverH );



        % Equation 2.11

        P_instant = (A_mn .* cos(L_m .*theta./thetamax).*sin(k_n.*zoverH) .*...

            (besseli(qm,k_n.*roverH) + alpha_mn.*besselk(qm,k_n.*roverH))...

           ./      subs(diff(besseli(qm,k_n.*roverH_)      +      alpha_mn.*besselk(qm,k_n.*roverH_),
roverH_),roverH_, aoverH)));



        Pxyz = Pxyz +  (P_instant);



    end

        m =mlarge

end



% get Vector P

 P = Pxyz;







% end
```

```
%%

% prepares and clears all existing variable(s) in workspace as well as command window

clear,clc

close all  % close all opened figures

%%



% Values to be varied: M and N

M = 10;

N = 10;



Npoints = 30;  % Number of discretized points to evaluate



thetamax = pi/4;

aoverb = 0.5;

aoverH = 0.1;



% Limits

thetamin = 0;      thetamax = 0;
```

```
zHmin = -1;     zHmax = 0;

rHmin = -1;     rHmax = 0;

% other parameters

mu = 0.5;



%% Figure 9 (a)



boverH =  [0.15 0.25 0.35 0.45 0.55]';



aoverb = aoverH ./boverH;



for i = 1: length(aoverb)

[Pxyz, P] = PressureImpulseFunction(thetamin, thetamax,zHmin,zHmax,...

                    mu, aoverb(i), aoverH, boverH(i), M, N, Npoints);



Pxyz_Variant{i} = Pxyz;



% MATRIX P
```

```
P_2{i} = P;

   i=i

end



%%

zoverH = linspace(zHmin, zHmax, Npoints)';  % limits for y/W

figure(1)

for  i = 1: length(aoverb)

plot(P_2{i},zoverH)

lengendcell2{i} = strcat('$b/H$ = ',num2str(boverH(i)));

hold on

end

hold off

ylabel('z/H')

xlabel('P/\rhoUH')

h1 = legend(lengendcell2{1:end});

set(h1, 'Interpreter', 'latex','Location','Best');
```

```
%% Figure 9 (b)



% update

mu = [0.2 0.4 0.6 0.8 1.0];

aoverb =0.5;

boverH = 0.3;



for i = 1: length(mu)

[Pxyz, P] = PressureImpulseFunction(thetamin, thetamax,zHmin,zHmax,...

                    mu(i), aoverb, aoverH, boverH, theta_max, M, N, Npoints);



Pxyz_Variant{i} = Pxyz;



% MATRIX P



P_3{i} = P;



end
```

```
zoverH = linspace(zHmin, zHmax, Npoints)';  % limits for y/W


figure(2)

for  i = 1: length(mu)

plot(P_3{i}, zoverH)

lengendcell2{i} = strcat('$\mu$ = ',num2str(mu(i)));

hold on

end

hold off

xlabel('P/\rhoUH')

ylabel('z/H')

% lengendcell2 = strcat('$w/H$ = ',string(num2cell(WoverH)));

h1 = legend({lengendcell2{1:end}});

set(h1, 'Interpreter', 'latex', 'Location','Best');


%%

%%
```

```
theta_max = pi/4;

aoverH = 0.1;



% Limits

% rHmin = aoverH;         rHmax = boverH;

thetamin = 0;       thetamax = 0;

zHmin = -1;      zHmax = 0;









%% Figure 10 (a)



% other parameters

aoverb = [0.17 0.33 0.50 0.67 0.83];

boverH = 0.3;

mu = 0.5;
```

```
for i = 1: length(aoverb)

[Pxyz, P] = PressureImpulseFunction(thetamin, thetamax,zHmin,zHmax,...

                    mu, aoverb(i), aoverH, boverH, theta_max, M, N, Npoints);



Pxyz_Variant{i} = Pxyz;



% MATRIX P



P_4{i} = P;



end



zoverH = linspace(zHmin, zHmax, Npoints)';  % limits for y/W

figure(3)

for  i = 1: length(aoverb)

plot(P_4{i},zoverH)

lengendcell2{i} = strcat('$a/b$ = ',num2str(aoverb(i)));

hold on
```

```
end

hold off

ylabel('z/H')

xlabel('P/\rhoUH')

h1 = legend(lengendcell2{1:end});

set(h1, 'Interpreter', 'latex','Location','Best');

%

%%

%% Figure 10 (b)



% update

mu = 0.5;

zHmin = -0.25*mu;   zHmax = -0.25*mu;

thetamin = -pi/4;      thetamax = pi/4;

thetamax = [pi/10 2*pi/10 3*pi/10 4*pi/10 pi/2];

aoverb =0.33;

boverH = 0.3;
```

```
for i = 1: length(thetamax)

[Pxyz, P] =  PressureImpulseFunction(thetamin, thetamax,zHmin,zHmax,...

                    mu, aoverb, aoverH, boverH, thetamax(i), M, N, Npoints);



Pxyz_Variant{i} = Pxyz;



% MATRIX P



P_5{i} = P;



end



theta_thetamax = linspace(thetamin/theta_max, thetamax/theta_max, Npoints)';  % limits



figure(4)

for  i = 1: length(theta_max_use)

plot(theta_thetamax, P_5{i})
```

```
lengendcell2{i} = strcat('$\theta_{max}$ = ',num2str(theta_max_use(i)/pi),'$\pi$');

hold on

end

hold off

ylabel('P/\rhoUH')

xlabel('\theta/\theta_max')

h1 = legend({lengendcell2{1:end}});

set(h1, 'Interpreter', 'latex', 'Location','Best');



%



%%

disp('Finished!')
```